UNIVERSIDADE DE SÃO PAULO

GENSMAC: A numerical method for solving unsteady non-newtonian free surface flows

MURILO F. TOMÉ
BRIAN DUFFY
SEAN MCKEE

Nº 08

NOTAS

Instituto de Ciências Matemáticas de São Carlos

Instituto de Ciências Matemáticas de São Carlos

ISSN - 0103-2577

GENSMAC: A numerical method for solving unsteady non-newtonian free surface flows

MURILO F. TOMÉ

BRIAN DUFFY

SEAN MCKEE

Nº 08

N O T A S D O I C M S C

Série Computação

São Carlos

abr. / 1994

GENSMAC: A Numerical Method for Solving Unsteady Non-Newtonian Free Surface Flows

Murilo F. Tome
Department of Computer Science and Statistics
ICMSC - USP de São Carlos

Brian Duffy and Sean McKee
Department of Mathematics
University of Strathclyde

Abstract

A numerical methodology for solving unsteady problems involving the generalized Newtonian model has been developed to investigate non-Newtonian free surface flows. It is an extension to the GENSMAC code which employs velocity and pressure to represent the fluid flow. A staggered grid is employed and marker particles are used to represent the fluid, providing immediate visualization of the moving free surface. The time-dependent Navier-Stokes equations and the full free surface stress conditions are considered. The technique has been applied to simulate the time-dependent extrudate-swell problem, showing the rheological features reported by existing methodologies for dealing with the steady state problem. Further results include the simulation of bluckling of Newtonian and non-Newtonian jets and injection molding in complex cavities. Furthermore, the technique is presented in such a way that any model relating the viscosity to the shear rate can be used.

1. INTRODUCTION

The Marker-and-Cell method was first introduced by Harlow and Welch [1] at the Los Alamos Scientific Laboratory in the early sixties. Since then it has been developed by several researchers [2], [3], [4], [5] (to cite a few) and a detailed description of the technique can be found in [2]. More recently Tomé and McKee [6] have developed the GENSMAC code, which is an updated Marker-and-Cell methodology for solving free surface flows in general domains. It solves the two-dimensional Navier-Stokes equations in Cartesian co-ordinates for an incompressible fluid. So far, the Marker-and-Cell type method has been applied to a wide range of flow problems, but as far as the Authors are aware, it has not been extended to cope with a non-Newtonian fluid. In this paper we describe modifications to GENSMAC in order to solve fluid flow problems for a specific non-Newtonian fluid, namely the generalized Newtonian model, in which the viscosity depends (in a prescribed way) on the local shear rate.

2. THE GENERALIZED NEWTONIAN MODEL

The balance laws for momentum and mass of an incompressible fluid of density ρ are

$$\rho \frac{D\mathbf{u}}{Dt} = \nabla \cdot \underline{\underline{\sigma}} + \rho \mathbf{g}, \qquad \nabla \cdot \mathbf{u} = 0, \tag{1}$$

where $\mathbf{u}(\mathbf{x},t)$, $\underline{\underline{\sigma}}(\mathbf{x},t)$ and $\mathbf{g}$ denote the fluid velocity, the stress tensor and gravitational acceleration, respectively. We shall consider flow of a generalized Newtonian fluid, with constitutive equations

$$\underline{\underline{\sigma}} = -p\underline{\underline{\mathbf{I}}} + \underline{\underline{\tau}}, \qquad \underline{\underline{\tau}} = 2\mu(q)\underline{\underline{\mathbf{d}}}, \tag{2}$$

where p is the fluid pressure, $\underline{\underline{\mathbf{I}}}$ is the identity tensor, $\underline{\underline{\tau}}$ is the extra-stress tensor, $\underline{\underline{\mathbf{d}}}$ is the rate-of-deformation tensor, given by

$$\underline{\underline{\mathbf{d}}} = \frac{1}{2}[(\nabla \mathbf{u}) + (\nabla \mathbf{u})^{\mathrm{T}}], \tag{3}$$

q is the local shear rate, defined by

$$q = \left(2\,\mathrm{tr}(\underline{\underline{\mathbf{d}}}^2)\right)^{1/2}, \tag{4}$$

and $\mu(q)$ is the apparent viscosity (a prescribed function of q). It is convenient to define also a kinematic viscosity $\nu = \mu/\rho$.

With (2) and (3), equation (1) becomes

$$\rho\frac{D\mathbf{u}}{Dt} = -\nabla p + \mu\nabla^2\mathbf{u} + (\nabla\mu)\cdot\left[(\nabla\mathbf{u}) + (\nabla\mathbf{u})^{\mathrm{T}}\right] + \rho\mathbf{g}, \qquad \nabla\cdot\mathbf{u} = 0. \tag{5}$$

We shall be concerned with unsteady free-surface flows of viscous fluid moving into a passive atmosphere (which we may take to be at zero pressure). In the absence of surface tension the normal and tangential components of stress must be continuous across any free surface, so that on such a surface

$$\mathbf{n}\cdot(\underline{\boldsymbol{\sigma}}\cdot\mathbf{n}) = 0 \quad \text{and} \quad \mathbf{m}\cdot(\underline{\boldsymbol{\sigma}}\cdot\mathbf{n}) = 0, \tag{6}$$

where $\mathbf{n}$ and $\mathbf{m}$ denote unit normal and tangent vectors to the surface.

We also have the boundary condition

$$\mathbf{u} = \mathbf{0} \quad \text{on any fixed boundary.} \tag{7}$$

Other boundary conditions, such as those at an entry or exit port to the computational domain, will be discussed later.

We consider two-dimensional flow, and use Cartesian coordinates Oxy, with $\mathbf{u} = u(x,y,t)\mathbf{i} + v(x,y,t)\mathbf{j}$. With L, U and ν_0 denoting 'typical' length, velocity and viscosity scales, we introduce the nondimensionalization

$$\mathbf{u} = U\bar{\mathbf{u}}, \quad \mathbf{x} = L\bar{\mathbf{x}}, \quad \nu = \nu_0\bar{\nu}, \quad q = \frac{U}{L}\bar{q}, \quad t = \frac{L}{U}\bar{t}, \quad p = \rho U^2\bar{p}, \quad \mathbf{g} = g\bar{\mathbf{g}},$$

where $g = |\mathbf{g}|$ (so that $\bar{\mathbf{g}}$ is a unit vector). For the sake of clarity we drop the overbars immediately. Then equation (5) can be cast in the forms

$$\frac{\partial\mathbf{u}}{\partial t} = -\nabla p + \mathbf{N}(\mathbf{u}) \tag{8}$$

and

$$\nabla\cdot\mathbf{u} = 0, \tag{9}$$

where $\mathbf{N}(\mathbf{u})$ has components

$$\begin{aligned} N_1 = &-\frac{\partial(u^2)}{\partial x} - \frac{\partial(uv)}{\partial y} + \frac{1}{Re}\nu(q)\frac{\partial}{\partial y}\left(\frac{\partial u}{\partial y} - \frac{\partial v}{\partial x}\right) \\ &+ \frac{1}{Re}\left[2\frac{\partial u}{\partial x}\frac{\partial\nu}{\partial x} + \left(\frac{\partial u}{\partial y} + \frac{\partial v}{\partial x}\right)\frac{\partial\nu}{\partial y}\right] + \frac{1}{F_r^2}g_x \end{aligned} \tag{10}$$

and

$$N_2 = -\frac{\partial(uv)}{\partial x} - \frac{\partial(v^2)}{\partial y} - \frac{1}{Re}\nu(q)\frac{\partial}{\partial x}\left(\frac{\partial u}{\partial y} - \frac{\partial v}{\partial x}\right)$$

$$+ \frac{1}{Re}\left[\left(\frac{\partial u}{\partial y} + \frac{\partial v}{\partial x}\right)\frac{\partial \nu}{\partial x} + 2\frac{\partial v}{\partial y}\frac{\partial \nu}{\partial y}\right] + \frac{1}{F_r^2}g_y, \tag{11}$$

with $\mathbf{g} = g_x\,\mathbf{i} + g_y\,\mathbf{j}$ and

$$q = \left[2\left(\frac{\partial u}{\partial x}\right)^2 + 2\left(\frac{\partial v}{\partial y}\right)^2 + \left(\frac{\partial u}{\partial y} + \frac{\partial v}{\partial x}\right)^2\right]^{1/2}, \tag{12}$$

$Re = UL/\nu_0$ and $F_r = U/\sqrt{Lg}$ denoting the associated Reynolds number and Froude number respectively. In obtaining (10) and (11), use has been made of the continuity condition (9). Equation (8) is in a form that is convenient for later use.

3. COMPUTATIONAL PROCEDURE

To solve equation (8) and (9) we employ a similar idea to that used in GENSMAC, namely, with marker particles used to represent the fluid, the equations are solved on a staggered grid at current time t, delivering the instantaneous value of $\mathbf{u}(\mathbf{x},t)$; the positions of the marker particles are then updated by solving $d\mathbf{x}/dt = \mathbf{u}$.

We suppose that at a given time, say t_0, the velocity field $\mathbf{u}(\mathbf{x},t_0)$ is known (satisfying the governing equations and boundary conditions, along with the pressure $p(\mathbf{x},t_0)$). The updated velocity field $\mathbf{u}(\mathbf{x},t)$, where $t = t_0 + \delta t$, is then determined as follows:

i) Calculate $q(\mathbf{x},t_0)$, and $\nu(q(\mathbf{x},t_0))$ using $\mathbf{u}(\mathbf{x},t_0)$.

ii) Let $\tilde{p}(\mathbf{x},t)$ be an arbitrary 'pressure' field that is consistent with the correct normal stress condition on the free surface at $t = t_0$.

iii) Calculate an intermediate 'velocity' field $\tilde{\mathbf{u}}(\mathbf{x},t)$ from

$$\frac{\partial \tilde{\mathbf{u}}}{\partial t} = -\nabla \tilde{p} + \mathbf{N}(\mathbf{u}), \tag{13}$$

with $\tilde{\mathbf{u}}(\mathbf{x},t_0) = \mathbf{u}(\mathbf{x},t_0)$, using the correct boundary conditions for $\mathbf{u}(\mathbf{x},t_0)$. Equation (13) is solved by means of an explicit Euler-type method.

Subtracting (13) from (8) we obtain

$$\frac{\partial}{\partial t}(\mathbf{u} - \tilde{\mathbf{u}}) = -\nabla(p - \tilde{p}), \tag{14}$$

so that $\nabla \times [(\partial/\partial t)(\mathbf{u} - \tilde{\mathbf{u}})] = \mathbf{0}$. Therefore $(\partial/\partial t)[\nabla \times (\mathbf{u} - \tilde{\mathbf{u}})] = \mathbf{0}$, which implies $\nabla \times (\mathbf{u} - \tilde{\mathbf{u}}) = \mathbf{f}(\mathbf{x})$ for some $\mathbf{f}(\mathbf{x})$. But $\mathbf{u} = \tilde{\mathbf{u}}$ at $t = t_0$, so that $\nabla \times \mathbf{u} = \nabla \times \tilde{\mathbf{u}}$ at $t = t_0$, implying $\mathbf{f}(\mathbf{x}) = \mathbf{0}$. Thus $\nabla \times (\mathbf{u} - \tilde{\mathbf{u}}) = \mathbf{0}$ for $t \in [t_0, t_0 + \delta t]$ (which shows that the 'vorticities' associated with $\tilde{\mathbf{u}}(\mathbf{x},t)$ and $\mathbf{u}(\mathbf{x},t)$ are the same). Therefore there exists a scalar function $\psi(\mathbf{x},t)$ such that

$$\mathbf{u}(\mathbf{x},t) - \tilde{\mathbf{u}}(\mathbf{x},t) = -\nabla \psi, \tag{15}$$

where, by continuity,

$$\nabla^2 \psi = \nabla \cdot \tilde{\mathbf{u}}(\mathbf{x},t). \tag{16}$$

iv) Solve the Poisson equation (16).

The appropriate boundary conditions for ψ are (see Tome and McKee [6])

$$\psi = 0 \qquad \text{on the free surface}$$

and

$$\frac{\partial \psi}{\partial n} = 0 \qquad \text{on mesh boundaries.}$$

These are treated using the accurate approximations detailed in Tome and McKee [6].

v) Obtain the updated velocity field $\mathbf{u}(\mathbf{x},t)$ from (15).

vi) Compute the pressure.

By (14) and (15) we have $p - \tilde{p} = \partial\psi/\partial t$, from which p is evaluated numerically as

$$p = \tilde{p} + \frac{\psi}{\delta t} \,. \tag{17}$$

Thus overall we essentially solve the momentum equations explicitly, and solve a sparse symmetric linear system (the discrete Poisson equation) for the 'velocity potential' ψ.

vii) Update the positions of the marker particles.

The last step is to move the marker particles to their new positions. These are virtual particles whose co-ordinates are stored and updated at the end of each calculational time-step by solving

$$\frac{dx}{dt} = u, \qquad \frac{dy}{dt} = v \tag{18}$$

by Euler's method. This provides a particle with its new co-ordinates, allowing us to determine whether or not it moves to a new computational cell, or indeed if it leaves the containment region throught an outlet.

Approximation of q on rigid boundaries.

When $\tilde{\mathbf{u}}$ is calculated from (13), the values of the shear rate q on rigid boundaries are required. These can be obtained as follows.

Let us consider a horizontal boundary $y = y_c$. If the no-slip condition is imposed on this boundary then

$$u(x, y_c) = 0 \qquad \text{and} \qquad v(x, y_c) = 0,$$

which gives

$$\frac{\partial u}{\partial x} = 0 \qquad \text{and} \qquad \frac{\partial v}{\partial x} = 0 \qquad \text{on} \quad y = y_c.$$

Introducing this into (12) we obtain

$$q(x, y_c) = \left[2\left(\frac{\partial v}{\partial y}\right)^2 + \left(\frac{\partial u}{\partial y}\right)^2\right]^{1/2}.$$

But conservation of mass implies $\partial v/\partial y = -\partial u/\partial x = 0$, so that, at a horizontal no-slip boundary, q reduces to

$$q(x, y_c) = \left|\frac{\partial u}{\partial y}\right|. \tag{19}$$

On the other hand, if $y = y_c$ is a free-slip boundary, defined by

$$v = 0 \qquad \text{and} \qquad \frac{\partial u}{\partial y} = 0 \qquad \text{on} \qquad y = y_c,$$

then

$$\frac{\partial v}{\partial x} = 0 \qquad \text{on} \qquad y = y_c,$$

so that from (12) and (9)

$$q(x, y_c) = 2\left|\frac{\partial v}{\partial y}\right| \tag{20}$$

on such a surface.

For a prescribed inflow or prescribed outflow through a horizontal boundary it is easily verified that q is also given by (19). For flow through a horizontal boundary $y = y_c$ at which the normal derivative of u vanishes (referred to as 'continuative' in [2]), q may be approximated by

$$q(x, y_c) = \left|\frac{\partial v}{\partial x}\right|. \tag{21}$$

Similarly, for a vertical boundary $x = x_c$ it can be shown that q may be approximated by

$$q(x_c, y) = \left|\frac{\partial v}{\partial x}\right| \tag{22}$$

when no-slip, prescribed inflow or prescribed outflow conditions are imposed, and may be approximated by

$$q(x_c, y) = 2\left|\frac{\partial u}{\partial x}\right| \tag{23}$$

if free-slip conditions are imposed. Also, it can be verified that for a continuative outflow on a vertical boundary, q is given by

$$q(x_c, y) = \left|\frac{\partial u}{\partial y}\right|. \tag{24}$$

The corresponding finite-difference versions of these equations will be given in the next Section.

4. FINITE DIFFERENCE APPROXIMATION

To solve equations (13), (16), (15), (17) and (18) we employ the following discrete approach.

A staggered grid is employed. A typical cell is as shown in figure 1.

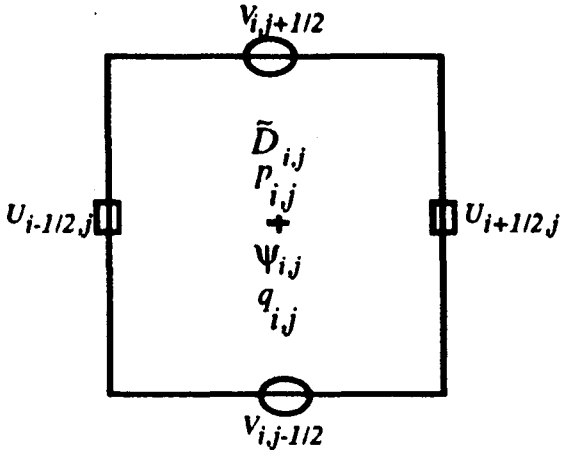

Fig. 1. Computational cell.

The variables, pressure $p_{i,j}$, the added velocity potential $\psi_{i,j}$, the divergence $\tilde{D}_{i,j}$ and the discrete shear rate $q_{i,j}$ are positioned at a cell centre while $u_{i,j}$ and $v_{i,j}$ are staggered by a translation of $\delta x/2$ and $\delta y/2$ respectively.

4.1 Cell Flagging

As the fluid is not stationary, a scheme to identify the fluid region and the free surface is employed. To accommodate this, the cells within the mesh are flagged according to whether they are

1. Boundary cells (B): Cells lying on or outside the boundary domain. They play a static role by prescribing the position of the fixed boundary.

2. Empty cells (E): Cells containing no fluid.

3. Full cells (F): Cells containing fluid with no adjacent empty cell on any of their faces.

4. Surface cells (S): Cells containing the free surface. These cells have at least one adjacent empty cell on one of their faces.

These definitions are illustrated in figure 2 for a typical case.

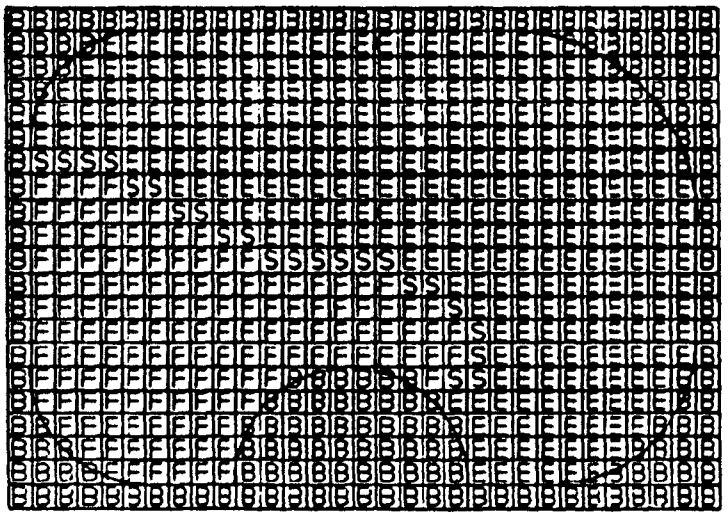

Fig. 2. Types of cells.

4.2 Basic Finite Difference Equations

The momentum equation (13) is discretised and applied at the u-nodes and v-nodes respectively. A forward difference is used to approximate the time derivatives while the linear spatial terms which do not contain ν-derivatives are approximated by central differences; for the convection terms in (10) and (11) the so-called ZIP form is adopted. This type of differencing requires the following approximations:

$$(u_{i,j})^2 = u_{i+\frac{1}{2},j}u_{i-\frac{1}{2}},$$

$$(v_{i,j})^2 = v_{i,j+\frac{1}{2}}v_{i,j-\frac{1}{2}}.$$

Thus, $\partial(u^2)/\partial x$ and $\partial(v^2)/\partial y$ in equations (10) and (11) are approximated by

$$\frac{u_{i+\frac{3}{2},j}u_{i+\frac{1}{2},j} - u_{i+\frac{1}{2},j}u_{i-\frac{1}{2},j}}{\delta x} \quad \text{and} \quad \frac{v_{i,j+\frac{3}{2}}v_{i,j+\frac{1}{2}} - v_{i,j+\frac{1}{2}}v_{i,j-\frac{1}{2}}}{\delta y}$$

respectively.

For the flux terms (uv), simple averages are performed, for instance:

$$(uv)_{i+\frac{1}{2},j+\frac{1}{2}} = \frac{(u_{i+\frac{1}{2},j} + u_{i+\frac{1}{2},j+1})}{2}\frac{(v_{i,j+\frac{1}{2}} + v_{i+1,j+\frac{1}{2}})}{2}.$$

Therefore the derivatives $\partial(uv)/\partial x$ and $\partial(uv)/\partial y$ are approximated by

$$\frac{\delta(uv)}{\delta x} = \frac{u_{i-\frac{1}{2},j+\frac{1}{2}} v_{i-\frac{1}{2},j+\frac{1}{2}} - u_{i+\frac{1}{2},j+\frac{1}{2}} v_{i+\frac{1}{2},j+\frac{1}{2}}}{\delta x}$$

and

$$\frac{\delta(uv)}{\delta y} = \frac{u_{i+\frac{1}{2},j-\frac{1}{2}} v_{i+\frac{1}{2},j-\frac{1}{2}} - u_{i+\frac{1}{2},j+\frac{1}{2}} v_{i+\frac{1}{2},j+\frac{1}{2}}}{\delta y}$$

respectively.

4.2.1. Computation of the Discrete Shear Rate - $q_{i,j}$.

To approximate the shear rate (12), we proceed as follows: the terms $\partial u/\partial x$ and $\partial v/\partial y$ are discretised by central differences, while for the terms $\partial u/\partial y$ and $\partial v/\partial x$ we first average u and v at the u and v-nodes and then apply central differences. For instance to discretise $\partial u/\partial y$ we compute $u_{i,j+\frac{1}{2}}$ and $u_{i,j-\frac{1}{2}}$ by averaging the four nearest u's and then take central differences with respect to y. To calculating the values of $u_{i,j+\frac{1}{2}}$ and $u_{i,j-\frac{1}{2}}$ let us consider figure 3a. Then it is easily seen that the values of $u_{i,j+\frac{1}{2}}$ and $u_{i,j-\frac{1}{2}}$ are given by

$$u_{i,j+\frac{1}{2}} := \frac{u_{i+\frac{1}{2},j+1} + u_{i-\frac{1}{2},j+1} + u_{i+\frac{1}{2},j} + u_{i-\frac{1}{2},j}}{4}$$

$$u_{i,j-\frac{1}{2}} := \frac{u_{i+\frac{1}{2},j} + u_{i-\frac{1}{2},j} + u_{i+\frac{1}{2},j-1} + u_{i-\frac{1}{2},j-1}}{4}$$

which gives

$$\frac{\partial u}{\partial y} = \frac{(u_{i,j+\frac{1}{2}} - u_{i,j-\frac{1}{2}})}{\delta y}.$$

The derivative $\partial v/\partial x$ is obtained similarly, namely

$$\frac{\partial v}{\partial x} = \frac{(v_{i+\frac{1}{2},j} - v_{i-\frac{1}{2},j})}{\delta x}$$

where

$$v_{i+\frac{1}{2},j} := \frac{v_{i+1,j+\frac{1}{2}} + v_{i,j+\frac{1}{2}} + v_{i+1,j-\frac{1}{2}} + v_{i,j-\frac{1}{2}}}{4}$$

$$v_{i-\frac{1}{2},j} := \frac{v_{i,j+\frac{1}{2}} + v_{i-1,j+\frac{1}{2}} + v_{i,j-\frac{1}{2}} + v_{i-1,j-\frac{1}{2}}}{4}.$$

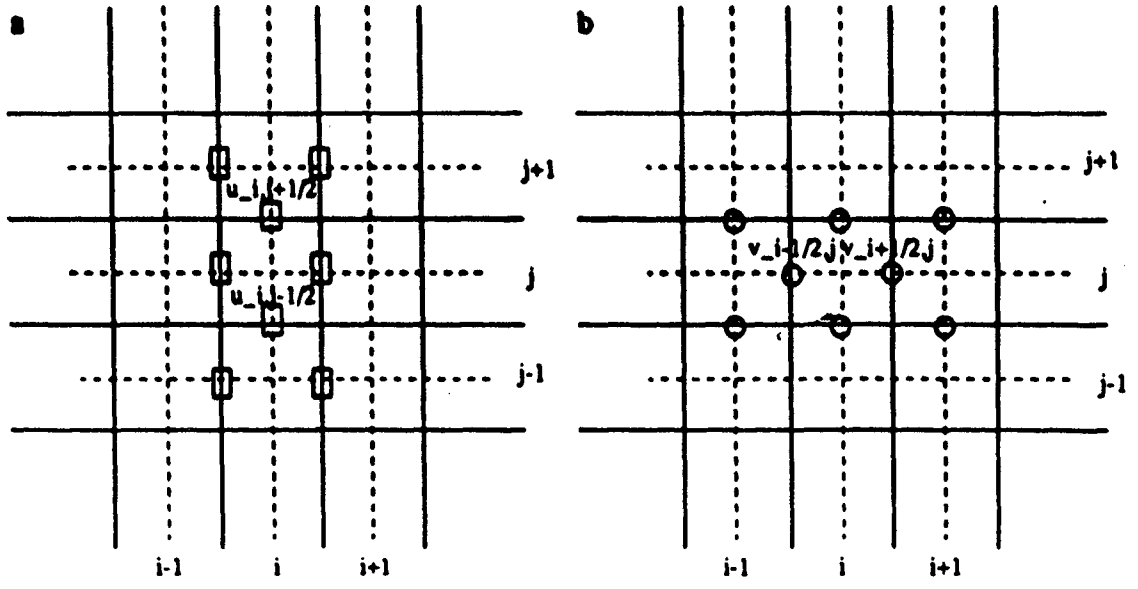

Fig. 3. Computation of u and v at v and u-nodes respectively.

With these approximations, the discrete shear rate, $q_{i,j}$ is given by

$$q_{i,j} = \left[2\left(\frac{u_{i+\frac{1}{2},j} - u_{i-\frac{1}{2},j}}{\delta x}\right)^2 + 2\left(\frac{v_{i,j+\frac{1}{2}} - v_{i,j-\frac{1}{2}}}{\delta y}\right)^2 + \left(\frac{u_{i+\frac{1}{2},j+1} + u_{i-\frac{1}{2},j+1} - u_{i+\frac{1}{2},j-1} - u_{i-\frac{1}{2},j-1}}{4\delta y} + \frac{v_{i+1,j+\frac{1}{2}} + v_{i+1,j-\frac{1}{2}} - v_{i-1,j+\frac{1}{2}} - v_{i-1,j-\frac{1}{2}}}{4\delta x}\right)^2\right]^{1/2}. \tag{25}$$

Once we compute $q_{i,j}$ the ν-derivatives are calculated as follows:

a) Approximation for the u-momentum equation

Here $\partial\nu/\partial x$ is approximated by central differences and $\partial\nu/\partial y$ is obtained by averaging, i.e.

$$\frac{\partial \nu}{\partial x} = \frac{\nu(q_{i+1,j}) - \nu(q_{i,j})}{\delta x}, \tag{26}$$

$$\left.\frac{\partial \nu}{\partial y}\right|_F = \frac{\nu(q_{i+\frac{1}{2},j+\frac{1}{2}}) - \nu(q_{i+\frac{1}{2},j-\frac{1}{2}})}{\delta y}, \tag{27}$$

where

$$q_{i+\frac{1}{2},j+\frac{1}{2}} = \frac{q_{i+1,j} + q_{i,j} + q_{i+1,j+1} + q_{i,j+1}}{4},$$

$$q_{i+\frac{1}{2},j-\frac{1}{2}} = \frac{q_{i,j} + q_{i+1,j} + q_{i,j-1} + q_{i+1,j-1}}{4}.$$

The subscript F denotes a cell which is not adjacent to the boundary. If the cell is adjacent to the boundary then (27) is replaced by

$$\left.\frac{\partial \nu}{\partial y}\right|_B = \frac{\nu(q_{i+\frac{1}{2},j+\frac{1}{2}})|_B - \nu(q_{i+\frac{1}{2},j-\frac{1}{2}})}{\delta y} \tag{28a}$$

or

$$\left.\frac{\partial \nu}{\partial y}\right|_B = \frac{\nu(q_{i+\frac{1}{2},j+\frac{1}{2}}) - \nu(q_{i+\frac{1}{2},j-\frac{1}{2}})|_B}{\delta y}. \tag{28b}$$

The choice in (28) is made depending upon which side of the cell is adjacent to the boundary, ie. top side or bottom side respectively. The values of

$$(q_{i+\frac{1}{2},j-\frac{1}{2}})|_B \qquad \text{and} \qquad (q_{i+\frac{1}{2},j+\frac{1}{2}})|_B$$

are computed by using the equations described in Section 3 according to the type of boundary condition imposed and will be given in Section 4.3 and 4.4.

For cells which are adjacent to empty cells (27) is replaced by

$$\left.\frac{\partial \nu}{\partial y}\right|_S = \frac{\nu(q_{i+\frac{1}{2},j+\frac{1}{2}})|_S - \nu(q_{i+\frac{1}{2},j-\frac{1}{2}})}{\delta y} \tag{29a}$$

or

$$\left.\frac{\partial \nu}{\partial y}\right|_S = \frac{\nu(q_{i+\frac{1}{2},j+\frac{1}{2}}) - \nu(q_{i+\frac{1}{2},j-\frac{1}{2}})|_S}{\delta y} \tag{29b}$$

The choice in (29) is made according to which side of the cell is adjacent to the empty cell, ie. top side or bottom side. The finite difference equations for

$$(q_{i+\frac{1}{2},j-\frac{1}{2}})|_S \qquad \text{and} \qquad (q_{i+\frac{1}{2},j+\frac{1}{2}})|_S$$

are obtained from the stress conditions on the free surface and will be given in Section 4.5.

b) Approximation for the v-momentum equation

Here the treatment for $\partial\nu/\partial x$ and $\partial\nu/\partial y$ is similar to above;

$$\left.\frac{\partial\nu}{\partial x}\right|_F = \frac{\nu(q_{i+\frac{1}{2},j+\frac{1}{2}}) - \nu(q_{i-\frac{1}{2},j+\frac{1}{2}})}{\delta x} \tag{30}$$

and

$$\frac{\partial\nu}{\partial y} = \frac{\nu(q_{i,j+1}) - \nu(q_{i,j})}{\delta y}. \tag{31}$$

where

$$q_{i-\frac{1}{2},j+\frac{1}{2}} = \frac{q_{i,j} + q_{i,j+1} + q_{i-1,j} + q_{i-1,j+1}}{4}.$$

For cells adjacent to the boundary, (30) is replaced by

$$\left.\frac{\partial\nu}{\partial x}\right|_B = \frac{\nu(q_{i+\frac{1}{2},j+\frac{1}{2}})|_B - \nu(q_{i-\frac{1}{2},j+\frac{1}{2}})}{\delta x} \tag{32a}$$

or

$$\left.\frac{\partial\nu}{\partial x}\right|_B = \frac{\nu(q_{i+\frac{1}{2},j+\frac{1}{2}}) - \nu(q_{i-\frac{1}{2},j+\frac{1}{2}})|_B}{\delta x} \tag{32b}$$

and for cells adjacent to empty cells (30) is given by

$$\left.\frac{\partial\nu}{\partial x}\right|_S = \frac{\nu(q_{i+\frac{1}{2},j+\frac{1}{2}})|_S - \nu(q_{i-\frac{1}{2},j+\frac{1}{2}})}{\delta x} \tag{33a}$$

or

$$\left.\frac{\partial\nu}{\partial x}\right|_S = \frac{\nu(q_{i+\frac{1}{2},j+\frac{1}{2}}) - \nu(q_{i-\frac{1}{2},j+\frac{1}{2}})|_S}{\delta x}. \tag{33b}$$

The expressions for calculating

$$(q_{i+\frac{1}{2},j+\frac{1}{2}})|_B, \quad (q_{i-\frac{1}{2},j+\frac{1}{2}})|_B, \quad (q_{i+\frac{1}{2},j+\frac{1}{2}})|_S, \quad \text{and} \quad (q_{i-\frac{1}{2},j+\frac{1}{2}})|_S$$

will be given in Sections 4.3, 4.4 and 4.5 respectively.

4.2.2 Computation of $\nu(q)$.

The function defining $\nu(q)$ can be any suitable function which describes the behaviour of ν as a function of q. For instance we employ the Cross equation (Barnes, Hutton and Walters [7])

$$\frac{\nu - \nu_\infty}{\nu_0 - \nu_\infty} = \frac{1}{\left(1 + (Kq)^m\right)} \tag{34}$$

where m, ν_0, ν_∞, and K are given positive constants.

The value of ν is required at u and v-nodes. This can be obtained from

$$\begin{aligned} \nu(q_{i+\frac{1}{2}j}) &= \nu_\infty + \frac{(\nu_0 - \nu_\infty)}{\left(1 + (Kq_{i+\frac{1}{2}j})^m\right)} \\ \nu(q_{ij+\frac{1}{2}}) &= \nu_\infty + \frac{(\nu_0 - \nu_\infty)}{\left(1 + (Kq_{ij+\frac{1}{2}})^m\right)} \end{aligned} \tag{35}$$

respectively. The values of $q_{i+\frac{1}{2}j}$ and $q_{ij+\frac{1}{2}}$ are easily obtained by averaging, namely:

$$q_{i+\frac{1}{2}j} = \frac{q_{i+1j} + q_{ij}}{2} \quad \text{and} \quad q_{ij+\frac{1}{2}} = \frac{q_{ij} + q_{ij+1}}{2} \,. \tag{36}$$

Now if we introduce the approximations made in this Section into the momentum equation (13) we obtain the following

$$\begin{aligned} &\frac{\tilde{u}^{n+1}_{i+\frac{1}{2}j} - u_{i+\frac{1}{2}j}}{\delta t} = \frac{u_{i+\frac{1}{2}j}u_{i-\frac{1}{2}j} - u_{i+\frac{1}{2}j}u_{i-\frac{1}{2}j}}{\delta x} - \frac{\tilde{p}_{i+1j} - \tilde{p}_{ij}}{\delta x} + (1/Fr^2)g_x \\ &+ (\frac{1}{Re})\nu(q_{i+\frac{1}{2}j})\Big[- \frac{(v_{i+1j+\frac{1}{2}} - v_{i+1j-\frac{1}{2}} - v_{ij+\frac{1}{2}} + v_{ij-\frac{1}{2}})}{\delta x \delta y} \\ &+ \frac{(u_{i+\frac{1}{2}j+1} + u_{i+\frac{1}{2}j-1} - 2u_{i+\frac{1}{2}j})}{\delta y^2}\Big] + \frac{u_{i+\frac{1}{2}j-\frac{1}{2}}v_{i+\frac{1}{2}j-\frac{1}{2}} - u_{i+\frac{1}{2}j+\frac{1}{2}}v_{i+\frac{1}{2}j+\frac{1}{2}}}{\delta y} \\ &+ (\frac{1}{Re})\Big[2\frac{(u_{i+\frac{1}{2}j} - u_{i-\frac{1}{2}j})}{2\delta x}(\frac{\partial \nu}{\partial x})_{i+\frac{1}{2}j} + \Big[\frac{u_{i+\frac{1}{2}j+1} - u_{i+\frac{1}{2}j-1}}{2\delta y} \\ &+ \frac{v_{i+1j+\frac{1}{2}} + v_{i+1j-\frac{1}{2}} - v_{ij+\frac{1}{2}} - v_{ij-\frac{1}{2}}}{2\delta x}\Big](\frac{\partial \nu}{\partial y})_{i+\frac{1}{2}j}\Big] \end{aligned} \tag{37}$$

where $\nu(q_{i+\frac{1}{2}j})$, $(\partial\nu/\partial x)_{i+\frac{1}{2}j}$, $(\partial\nu/\partial y)_{i+\frac{1}{2}j}$, and $q_{i+\frac{1}{2}j}$ are obtained from (35), (26), (27), and (36) respectively .

$$\frac{\tilde{v}^{n+1}_{i,j+\frac{1}{2}} - v_{i,j+\frac{1}{2}}}{\delta t} = \frac{v_{i,j+\frac{1}{2}} v_{i,j-\frac{1}{2}} - v_{i,j+\frac{1}{2}} v_{i,j+\frac{1}{2}}}{\delta y} - \frac{\tilde{p}_{i,j+1} - \tilde{p}_{i,j}}{\delta y} + (1/Fr^2) g_y$$

$$- (\frac{1}{Re}) \nu(q_{i,j+\frac{1}{2}}) \Bigg[\frac{(u_{i+\frac{1}{2},j+1} - u_{i+\frac{1}{2},j} - u_{i-\frac{1}{2},j+1} + u_{i-\frac{1}{2},j})}{\delta x \delta y}$$

$$+ \frac{(2v_{i,j+\frac{1}{2}} - v_{i+1,j+\frac{1}{2}} - v_{i-1,j+\frac{1}{2}})}{\delta x^2} \Bigg] + \frac{u_{i-\frac{1}{2},j+\frac{1}{2}} v_{i-\frac{1}{2},j+\frac{1}{2}} - u_{i+\frac{1}{2},j+\frac{1}{2}} v_{i+\frac{1}{2},j+\frac{1}{2}}}{\delta x} \qquad (38)$$

$$+ (\frac{1}{Re}) \Bigg[\Bigg[\frac{u_{i+\frac{1}{2},j+1} + u_{i-\frac{1}{2},j+1} - u_{i+\frac{1}{2},j} - u_{i-\frac{1}{2},j}}{2\delta y}$$

$$+ \frac{v_{i+1,j+\frac{1}{2}} - v_{i-1,j+\frac{1}{2}}}{2\delta x} \Bigg] (\frac{\partial \nu}{\partial x})_{i,j+\frac{1}{2}} + 2 \frac{(v_{i,j+\frac{1}{2}} - v_{i,j-\frac{1}{2}})}{2\delta y} (\frac{\partial \nu}{\partial y})_{i,j+\frac{1}{2}} \Bigg]$$

where $\nu(q_{i,j+\frac{1}{2}})$, $(\partial\nu/\partial x)_{i,j+\frac{1}{2}}$, $(\partial\nu/\partial y)_{i,j+\frac{1}{2}}$, and $q_{i,j+\frac{1}{2}}$ are obtained from (35), (30), (31) and (36) respectively. The superscript n has been dropped for clarity.

The Poisson equation (16) is discretised at cell centres using the five point Laplacian which can be written as

$$4\psi_{i,j} - \psi_{i+1,j} - \psi_{i-1,j} - \psi_{i,j+1} - \psi_{i,j-1} = -h^2 \tilde{D}_{i,j} \qquad (39)$$

where

$$\tilde{D}_{i,j} = \frac{\tilde{u}_{i+\frac{1}{2},j} - \tilde{u}_{i-\frac{1}{2},j}}{\delta x} + \frac{\tilde{v}_{i,j+\frac{1}{2}} - \tilde{v}_{i,j-\frac{1}{2}}}{\delta y}$$

and

h denotes the grid size (assuming $\delta x = \delta y$).

4.3 Boundary Conditions

The various types of boundary conditions mentioned in Section 3.2 may be applied at the walls of the computing mesh. The finite difference form of those conditions for a left wall will be given here; the treatment of other wall positions is similiar. With reference to figure 4 the indices $i+1, j$ refer to a cell inside the fluid domain and i, j refer to the cell lying just outside the fluid domain.

a) Inflow/Outflow boundaries

Inflow and outflow boundaries can be specified as either normal and/or tangential velocitites at the boundary. In addition, normal derivative boundary conditions can be specified at the outflow. For simplicity, it will be assumed that the inflow and outflow coincide with cell boundaries. These types of boundary conditions can be given as follows:

i) INFLOW : Fluid flows in through a segment of the boundary at a prescribed rate. As in GENSMAC, the desired inflow is constant and marker particles are inserted through the wall to represent the incoming fluid. With reference to figure 4 this can be stated as

$$u_{i+\frac{1}{2},j} = U_i,$$

$$v_{i,j+\frac{1}{2}} = -v_{i+1,j+\frac{1}{2}},$$

$$v_{i,j-\frac{1}{2}} = -v_{i+1,j-\frac{1}{2}},$$

$$\psi_{i,j} = \psi_{i+1,j}.$$

The shear rate (22) at the boundary is computed at mesh corners and is given by

$$q_{i+\frac{1}{2},j+\frac{1}{2}}\Big|_B = \frac{2|v_{i+1,j+\frac{1}{2}}|}{\delta x}.$$

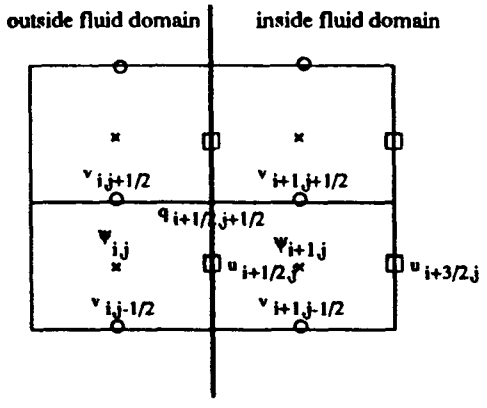

Fig. 4. Variable positions for a left wall.

ii) OUTFLOW : Fluid flows out through a segment of the boundary and marker particles are destroyed as they cross the boundary. The boundary conditions can be of two types: prescribed and continuative. With prescribed outflows the fluid is removed from the domain at a constant prescribed rate while with continuative outflows the fluid flows out of the domain in such away

that there is no rate of spatial change in the velocity. With reference to figure 4 this can be stated as:

Prescribed outflow

$$u_{i+\frac{1}{2}j} = U_o,$$

$$v_{ij+\frac{1}{2}} = -v_{i+1j+\frac{1}{2}},$$

$$v_{ij-\frac{1}{2}} = -v_{i+1j-\frac{1}{2}},$$

$$\psi_{ij} = \psi_{i+1j}.$$

The shear rate (22) is computed at mesh corners and is given by

$$q_{i+\frac{1}{2}j+\frac{1}{2}}\Big|_B = \frac{2|v_{i+1j+\frac{1}{2}}|}{\delta x}.$$

Continuative outflow

$$u_{i+\frac{1}{2}j} = \bar{u}_{i+\frac{3}{2}j} + \frac{\psi_{i+1j}}{\delta x},$$

$$v_{ij+\frac{1}{2}} = v_{i+1j+\frac{1}{2}},$$

$$v_{ij-\frac{1}{2}} = v_{i+1j-\frac{1}{2}},$$

$$\psi_{ij} = 0.$$

The shear rate (24) is approximated by

$$q_{i+\frac{1}{2}j+\frac{1}{2}}\Big|_B = \frac{|u_{i+\frac{1}{2}j+1} - u_{i+\frac{1}{2}j}|}{\delta y}.$$

b) Free-Slip Boundary

The free-slip condition may represent a line of symmetry or a surface which exerts no drag on a fluid. This is accomplished by requiring the normal velocity and the normal derivative of the tangential velocity to vanish on the boundary. If the boundary coincides with mesh lines then the free-slip condition can be applied directly. For a left wall (see figure 4) this condition can be represented by

$$u_{i+\frac{1}{2}j} = 0,$$

$$v_{ij+\frac{1}{2}} = v_{i+1j+\frac{1}{2}},$$

$$v_{ij-\frac{1}{2}} = v_{i+1j-\frac{1}{2}},$$

$$\psi_{ij} = \psi_{i+1j}.$$

The shear rate (23) is approximated by

$$q_{i+\frac{1}{2}j+\frac{1}{2}}\Big|_B = \frac{|u_{i+\frac{1}{2}j} + u_{i+\frac{1}{2}j+1}|}{\delta x}.$$

c) No-Slip Boundary

A no-slip boundary represents a viscous boundary that exerts a drag upon the fluid. This is accomplished by making the normal and tangential velocities zero at the wall. In terms of finite differences this is represented by

$$u_{i+\frac{1}{2}j} = 0,$$

$$v_{ij+\frac{1}{2}} = -v_{i+1j+\frac{1}{2}},$$

$$v_{ij-\frac{1}{2}} = -v_{i+1j-\frac{1}{2}},$$

$$\psi_{ij} = \psi_{i+1j}.$$

The shear rate (22) is approximated by

$$q_{i+\frac{1}{2}j+\frac{1}{2}}\Big|_B = \frac{2|v_{i+1j+\frac{1}{2}}|}{\delta x}.$$

4.4 Curved Boundary Treatment

A methodology for treating curved boundaries when the no-slip condition is imposed has been developed during the construction of the GENSMAC code in order to be able to deal with free surface flows in arbitrary domains. The same methodology is employed for solving the generalized Newtonian fluid for which we give a brief description. For details see Tome and McKee [6].

4.4.1 Virtual Boundary Definition

For a rectangular domain, no problems arise when the finite difference equations (37) and (38) are applied at nodes near the boundary because these coincide with cell edges; however, a curved boundary will not in general coincide with cell edges and any interpolation procedure must accord with the staggered grid. This can be achieved first by determining where the curved boundary cuts the cell edges and then flagging this cell as a B-cell or not. Let us assume that the cells are sufficiently small so that the curved boundary will cut a cell at two points. Then all the possible configurations of cells cut by the curved boundary can be classified into one of the two groups: cell cut on two adjacents sides (corner cell) and cells cut on sides which are opposite to one another (edge cell). Figure 5 displays examples of such cells.

Among the corner cells and the edge cells we consider the ones such as shown in figure 5a and 5c to be interior cells (ie. F, S, or E) because only a small part of these cells is occupied by the rigid boundary while we consider the other cells such as in figure 5b and 5d to belong to the curved boundary and special treatment is then required for these cases. The criterium for deciding which of these cells belong to the curved boundary is given in Tome and McKee [6] and is not given here. Thus, after the flagging is performed the boundary is approximated by piece-wise continuous mesh lines. Figure 6 displays an example of such a boundary. The approximated boundary which we call "virtual boundary", is the reference boundary for the Poisson equation (16).

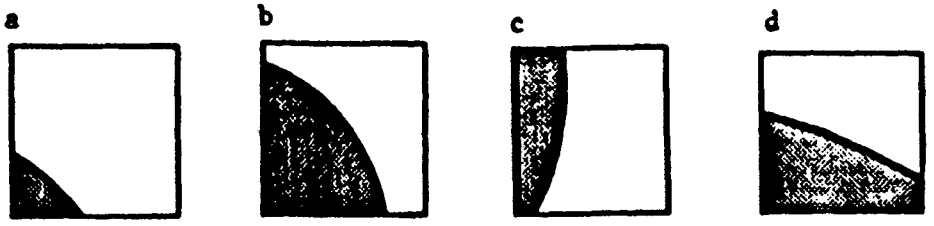

Fig. 5. Types of cells cut by a curved boundary: Corner and Edge cells.

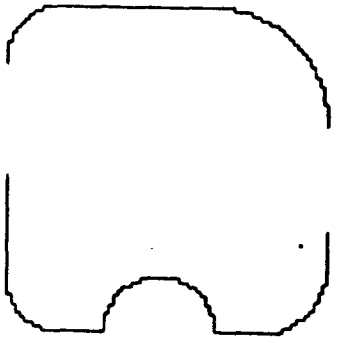

Fig. 6. Virtual boundary.

4.4.2 Boundary Conditions on Curved Surfaces

When the discretised momentum equations (37) and (38) are applied at nodes adjacents to the virtual boundary, the u and v values at boundary cell faces are required. If no-slip conditions are applied on the curved boundary, these values can be estimated in terms of functions values at internal nodes by linear (bilinear) interpolation.

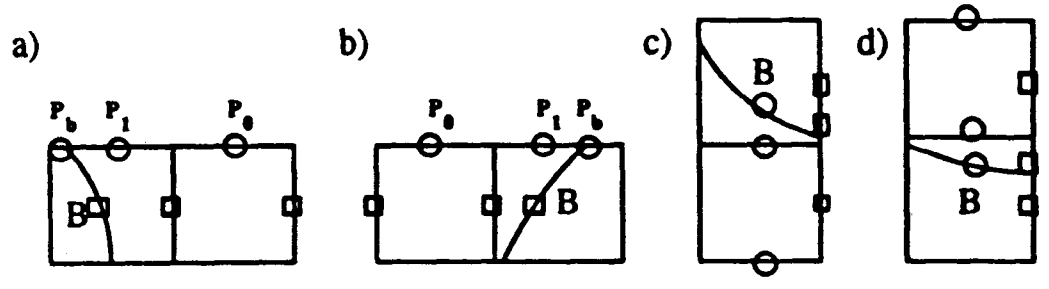

Fig. 7. Configurations of B-cells with only one side open to interior cell.

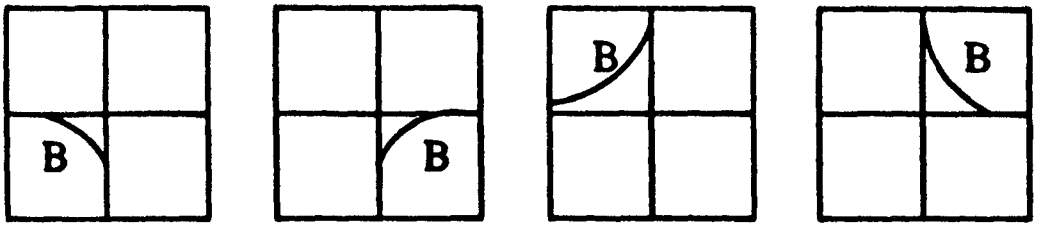

Fig. 8. Configurations of B-cells with two sides open to interior cells.

It can be seen that the boundary cells may have one or two sides open to interior cells, as shown in figure 7 and in figure 8. Thus, if a B-cell has one open side the u, v-values are computed by using linear interpolation while for B-cells having two sides open a bilinear interpolation is employed. For details of the interpolation formulae see [6].

4.4.3 Computation of q on Boundary Cell Corners

When computing the viscosity derivatives in (28) and (32) the values of q at boundary cell corners are required. This is obtained by making finite differences approximations to (12) by considering two cases:

a) B-cells with only one side contiguous with interior cells

For these cells we assume that the curved boundary can be approximated by either a horizontal or vertical boundary in which case we compute $q_{i+\frac{1}{2},j+\frac{1}{2}}$ by using (19) or (22) respectively. For instance, in the case of a B-cell having only the right side contiguous with a interior cell as in figure 9, the value of $q_{i+\frac{1}{2},j+\frac{1}{2}}$ is obtained by

$$q_{i+\frac{1}{2},j+\frac{1}{2}} = \frac{v_{i,j+\frac{1}{2}} - v_{i-1,j+\frac{1}{2}}}{\delta x} .$$

Other configurations of B-cells having only one side contiguous with a interior is treated similarly.

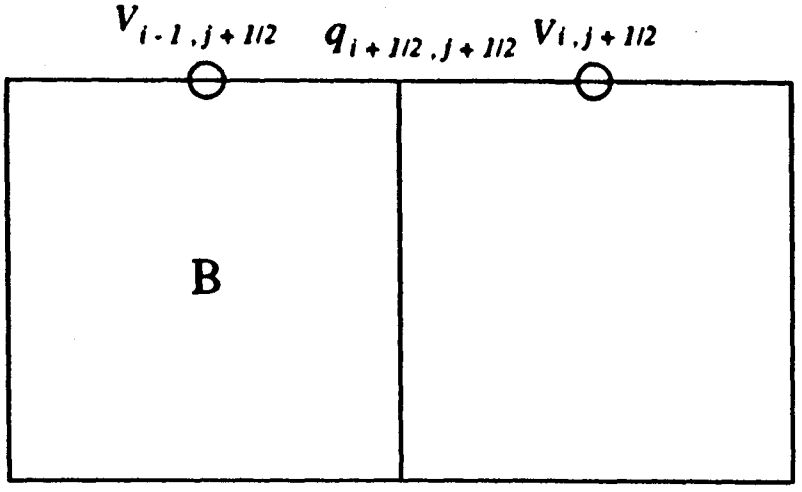

Fig. 9. B-cell with the right side contiguous with a interior cell

b) B-cells with two sides contiguous with interior cells

For these cells, the value of $q_{i+\frac{1}{2},j+\frac{1}{2}}$ is obtained by making finite difference approximations to (12). For example, if we consider the B-cell as in figure 10 then the value of $q_{i+\frac{1}{2},j+\frac{1}{2}}$ can be obtained from

$$
\begin{aligned}
q_{i+\frac{1}{2},j+\frac{1}{2}} = \Bigg[& 2\left(\frac{u_{i+\frac{1}{2},j+1}+u_{i+\frac{1}{2},j}-u_{i-\frac{1}{2},j+1}-u_{i-\frac{1}{2},j}}{2\delta x}\right)^2 \\
& + 2\left(\frac{v_{i,j+\frac{3}{2}}+v_{i-1,j+\frac{3}{2}}-v_{i,j+\frac{1}{2}}-v_{i-1,j+\frac{1}{2}}}{2\delta y}\right)^2 \\
& + \left(\frac{u_{i-\frac{1}{2},j+1}-u_{i-\frac{1}{2},j}}{\delta y}+\frac{v_{i,j+\frac{1}{2}}-v_{i-1,j+\frac{1}{2}}}{\delta x}\right)^2 \Bigg]^{1/2} .
\end{aligned}
$$

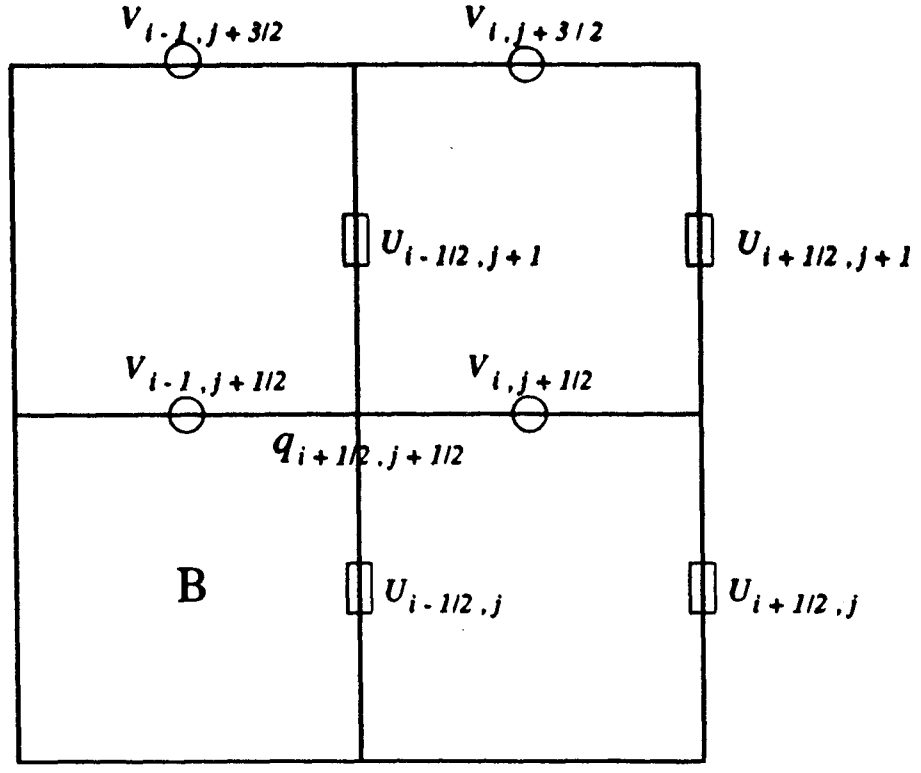

Fig. 10. B-cell having the right and top sides contiguous with interior cells

For other configurations of B-cells having two sides contiguous with interior cells the value of $q_{i+\frac{1}{2},j+\frac{1}{2}}$ is obtained similarly.

4.5 Free Surface Stress Conditions

The treatment of the free surface stress conditions is analogous to that considered in GENSMAC [6]. The stress conditions are approximated by local finite differences by assuming three types of surface orientation: horizontal, vertical and 45^0 sloped surface, as follows.

Let us assume that the grid size is small enough so that the surface will intercept the mesh cell at two edges. Then, equation (6) can be simplified by considering three cases:

a) Surface cells (S) with only one side open to an empty cell (E).

For these cells we assume that the surface will be either horizontal or vertical in which case (6) reduces to

$$p - \frac{2}{Re}\nu(q)\left(\frac{\partial u_n}{\partial n}\right) = 0 \tag{40}$$

$$\frac{\partial u}{\partial y} + \frac{\partial v}{\partial x} = 0 \tag{41}$$

where n is either the x-direction or the y-direction.

Finite difference approximations for (40) are easily obtained. For instance, if we consider the surface cells in figure 11, the corresponding finite diference approximation for (40) is

$$p_{i,j} = (2/Re)\nu(q_{i,j})\left(\frac{u_{i+\frac{1}{2},j} - u_{i-\frac{1}{2},j}}{\delta x}\right).$$

while the tangential stress (41) is approximated by

$$v_{i+1,j+\frac{1}{2}} = v_{i,j+\frac{1}{2}} - \frac{\delta x}{\delta y}(u_{i+\frac{1}{2},j+1} - u_{i+\frac{1}{2},j}).$$

The shear rate $q_{i,j}$ is computed from (12) which in this case reduces to

$$q = 2\left|\frac{\partial u}{\partial n}\right|. \tag{42}$$

For the surface cells in figure 5, q can be approximated by

$$q_{i,j} = 2\frac{\left|u_{i+\frac{1}{2},j} - u_{i-\frac{1}{2},j}\right|}{\delta x}.$$

Once we compute $q_{i,j}$ the value of $\nu(q_{i,j})$ is calculated by

$$\nu(q_{i,j}) = \nu_\infty + \frac{(\nu_0 - \nu_\infty)}{\left(1 + (Kq_{i,j})^m\right)}. \tag{43}$$

When calculating the q-derivatives in (29) and (30) the values of q at the surface cell corners are required. This can be obtained by making finite difference approximations to (42) at the cell corners, namely

$$q_{i+\frac{1}{2},j+\frac{1}{2}}\Big|_S = 2\frac{\left|u_{i+\frac{1}{2},j+\frac{1}{2}} - u_{i-\frac{1}{2},j+\frac{1}{2}}\right|}{\delta x}$$

where

$$u_{i+\frac{1}{2},j+\frac{1}{2}} = \frac{u_{i+\frac{1}{2},j+1} + u_{i+\frac{1}{2},j}}{2} \qquad \text{and} \qquad u_{i-\frac{1}{2},j+\frac{1}{2}} = \frac{u_{i-\frac{1}{2},j+1} + u_{i-\frac{1}{2},j}}{2}.$$

Other types of surface cells with only one side adjacent to empty cells are treated similarly.

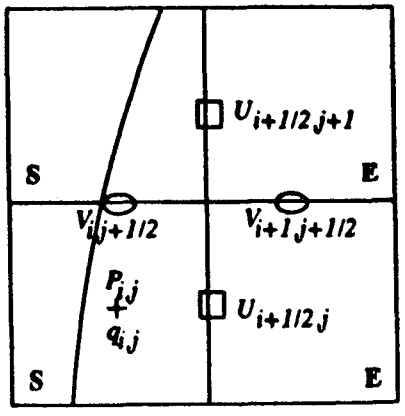

Fig. 11. Surface Cell with the right side contiguous to an empty cell.

b) Surface cells with two adjacent sides contiguous with empty cells

For these cells we assume that the outward normal direction lies at 45° between the open sides. In this case the stress conditions (6) reduce to

$$p = \pm(1/Re)\nu(q)\left(\frac{\partial u}{\partial y} + \frac{\partial v}{\partial x}\right) \tag{44}$$

$$\frac{\partial u}{\partial x} - \frac{\partial v}{\partial y} = 0. \tag{45}$$

The sign in (44) is chosen to be the sign of $n_x n_y$. For example, let us consider the surface cell in figure 12. Thus a finite difference approximation for (44) would be

$$p_{i,j} = (Re/2)\nu(q_{i,j})\left[\frac{u_{i+\frac{1}{2}j} + u_{i-\frac{1}{2}j} - u_{i+\frac{1}{2}j-1} - u_{i-\frac{1}{2}j-1}}{\delta y}\right.$$
$$\left. + \frac{v_{i,j+\frac{1}{2}} + v_{i,j-\frac{1}{2}} - v_{i-1,j+\frac{1}{2}} - v_{i-1,j-\frac{1}{2}}}{\delta x}\right]. \tag{46}$$

For the tangential stress (45) we require $\partial u/\partial x$ and $\partial v/\partial y$ to vanish separately. The reason for doing this is that the mass conservation equation is also satisfied for these cells. For example, for the surface cell as shown in figure 12 we set

$$u_{i+\frac{1}{2}j} = u_{i-\frac{1}{2}j} \qquad \text{and} \qquad v_{i,j+\frac{1}{2}} = v_{i,j-\frac{1}{2}}.$$

The shear rate (12), on these cells, reduces to

$$q = \left|\frac{\partial u}{\partial y} + \frac{\partial v}{\partial x}\right|$$

which can be approximated in the same way as in (45), namely

$$q_{i,j} = \frac{1}{2}\left|\frac{u_{i+\frac{1}{2}j} + u_{i-\frac{1}{2}j} - u_{i+\frac{1}{2}j-1} - u_{i-\frac{1}{2}j-1}}{\delta y}\right.$$

$$\left. + \frac{v_{ij+\frac{1}{2}} + v_{ij-\frac{1}{2}} - v_{i-1j+\frac{1}{2}} - v_{i-1j-\frac{1}{2}}}{\delta x}\right|.$$

Once we compute $q_{i,j}$ the value of $\nu(q_{i,j})$ is calculated by (43).

For other configurations of surface cells with two adjacent sides contiguous with empty cells the finite difference approximations are obtained similarly.

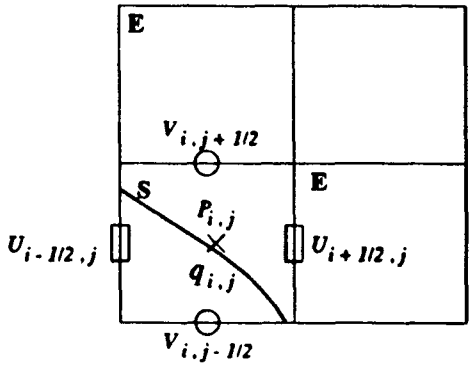

Fig. 12. Surface Cell with the top and right sides contiguous to empty cells.

c) Surface cell with two sides, which are opposite to each other, contiguous with empty cells.

For these cells the pressure is set to zero and one velocity is adjusted so that $\nabla.\mathbf{u} = 0$ in the surface cell. The shear rate $q_{i,j}$ is set to zero in these cells. If such cells arise it suggests that the grid should be refined.

4.6 Time-Stepping Control

A time step procedure is employed which optimizes the time-step size at each calculational cycle. It is based on two stability restrictions:

1. No particles should cross more than one cell boundary interval in a given time interval, i.e. that

$$\delta t < \frac{\delta x}{|u|} \quad \text{and} \quad \delta t < \frac{\delta y}{|v|}. \tag{47}$$

2. The second stability restriction is due to the explicity discretisation of the momentum equations and involves the Reynolds number and the viscosity:

$$\delta t < \frac{\delta x^2 \delta y^2}{\delta x^2 + \delta y^2} \frac{Re}{2} (\frac{1}{\nu(q)}). \tag{48}$$

Thus to satisfy (47) it is sufficient that

$$\delta t < \frac{\delta x}{|U_{max}|} \qquad \text{and} \qquad \delta t < \frac{\delta y}{|V_{max}|} \tag{49}$$

where U_{max}, V_{max} are the maximum of values of u and v respectively. In order that (48) be satisfied it is required that

$$\delta t < \frac{\delta x^2 \delta y^2}{\delta x^2 + \delta y^2} \frac{Re}{2} (\frac{1}{\nu_{max}}) \tag{50}$$

where

$$\nu_{max} = max\{ \nu_{i,j} \}.$$

The implementation of (49) and (50) has been performed in essentially the same way as in GENSMAC [6].

4.7 The Poisson Solver

The discrete Poisson equation (39) gives rise to a linear system which is the same as in the Newtonian case. The conjugate gradient solver as implemented in GENSMAC [6] is employed to solve this linear system.

4.8 Particle Movement

Marker particles are used to represent the fluid. Their essential task is to provide the position of the moving free surface so that the configuration of the surface cells can be determined. They are updated at the end of each calculational time-step so as to provide the dynamics of the fluid

motion. The new particle coordinates are found by solving (18) using Euler's method. Thus, after the velocity field is updated, the particles are moved according to

$$x_p^{n+1} = x_p + u_p \delta t^{n+1}$$

$$y_p^{n+1} = y_p + v_p \delta t^{n+1}$$

where (x_p, y_p) is the current particle position, δt^{n+1} is the actual time-step employed and (x_p^{n+1}, y_p^{n+1}) its updated position. The velocities u_p, v_p are computed by using an area weighting scheme involving the four nearest u, v velocities respectively. For details see [6], [2].

5. CALCULATIONAL EXAMPLES AND APPLICATIONS

The finite differences equations described in Section 4 were incorporated into the GENSMAC code in order to allow the investigation of incompressible free surface flows of non-Newtonian fluids. To demonstrate that the technique described in this paper can indeed cope with shear thinning viscosity we present three known problems which compared with the respective Newtonian case show non-Newtonian behaviour. These are discussed next.

5.1 Numerical Simulation of the Transient Die Swell of a Planar Jet

The first calculation presents a simulation of the flow of a planar jet emerging from the die which exhibits the characteristic phenomenon known as 'extrudate swell' or 'jet swell'. This problem has attracted the attention of many researchers and numerous techniques for simulating the jet swell of a non-Newtonian fluid (eg. [8], [9], as well as a Newtonian fluid (eg. [10], 11]) have been developed. However the procedures employed so far have only, to the Authors's knowledge, been able to accommodate stationary regimes and often neglecting the inertia terms by considering the case of very viscous jets. Due to the complexity of the flow domain, the most common technique has been that of finite element (eg. [12]) but finite differences have also been employed (eg. [13]).

Problem Description.

We consider the time-dependent flow of a two-dimensional jet flowing through a slit with a constant input velocity and then extrudatet into the air. If on the slit walls the no-slip condition is imposed this will affect the constant input velocity resulting in an approximate parabolic profile at the slit exit where, under certain conditions, the jet might be expected to exhibit the phenomenon of swelling. Figure 13 displays the geometry and the boundary conditions associated with the die-swell problem.

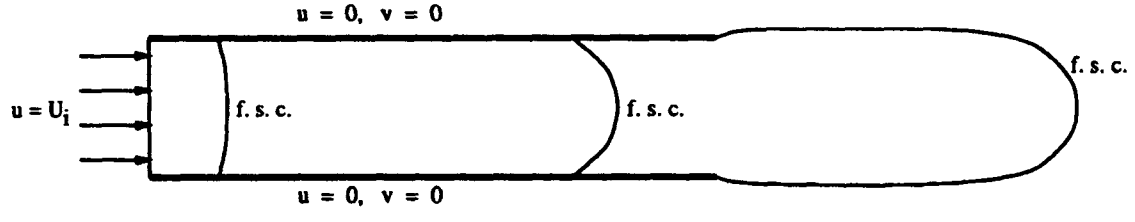

Fig. 13. The die-swell problem.

The input velocity is set to $U_i = 5\ m/s$ and the slit diameter is $D = 1\ cm$. The length of the slit was set to 3 cm which should be long enough for the velocity profile to become similar to parabolic at the slit exit. A continuative outflow is set at 6 cm from the slit exit. The scaling parameters were taken to be $L = D$ and $U = U_i$ (inlet velocity) which give a Reynolds number of $Re = 1.0$. Gravity was neglected as $1/F_r^2 \approx 0.003$.

The viscosity is defined by (34) and we use the following values for the constants:

$$\begin{aligned} \nu_\infty &= 0.001\ m^2/s, \\ \nu_0 &= 0.050\ m^2/s, \\ m &= 1.0\ . \end{aligned}$$

In order to observe non-Newtonian behaviour we have run this problem for 3 differents values of K namely: $K = 0.15$, 0.75 and 1.5 respectively.

Figure 14 displays the fluid configuration at a particular time for the differents values of K and figure 15 shows the fluid configuration at different times for $K = 1.5$

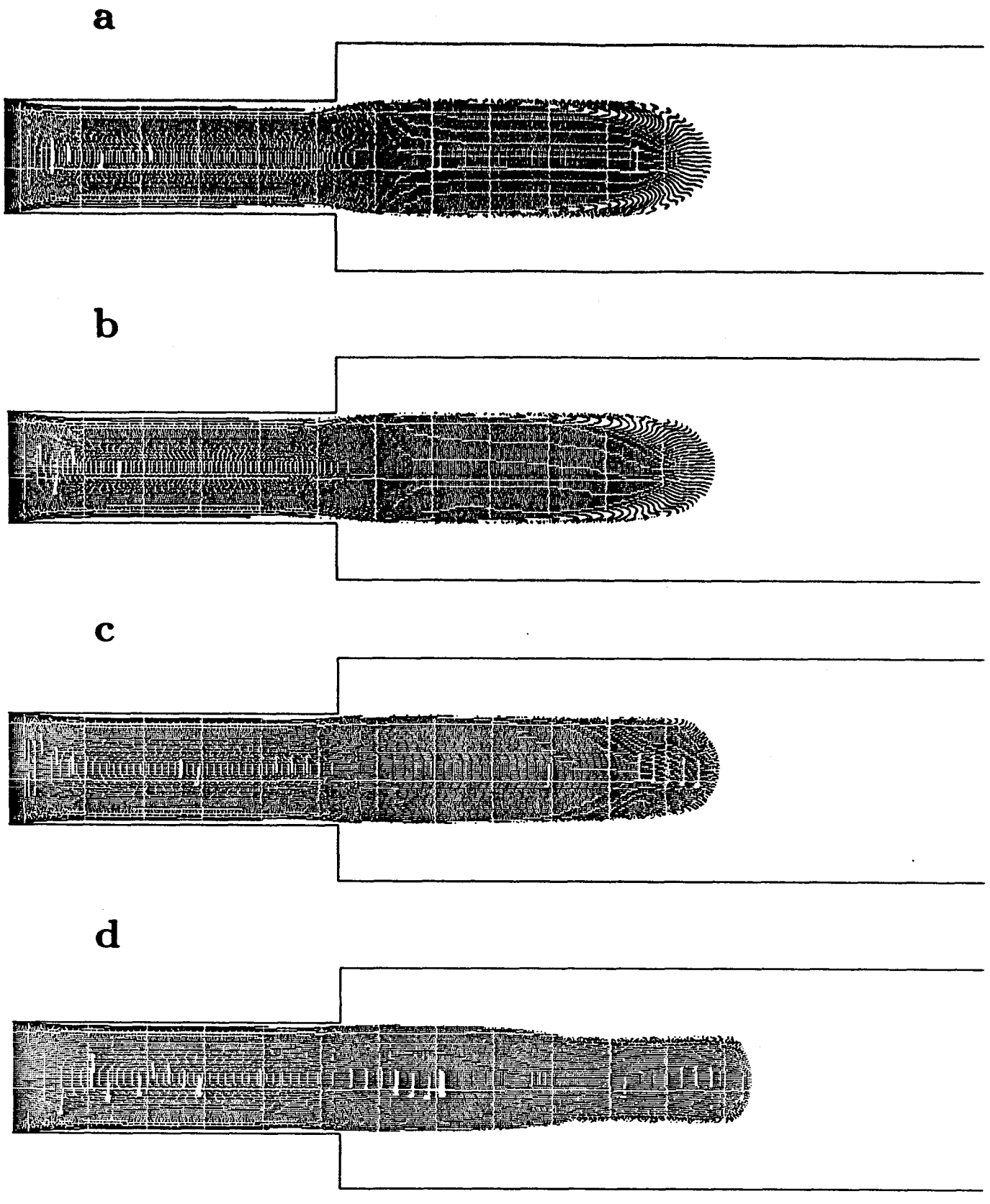

Fig. 14. Extrudate swell of Newtonian and non-Newtonian jets at t = 6.250 for differents values of K. - a: K = 0.0, b: K = 0.15, c: K = 0.75 and d: K = 1.5.

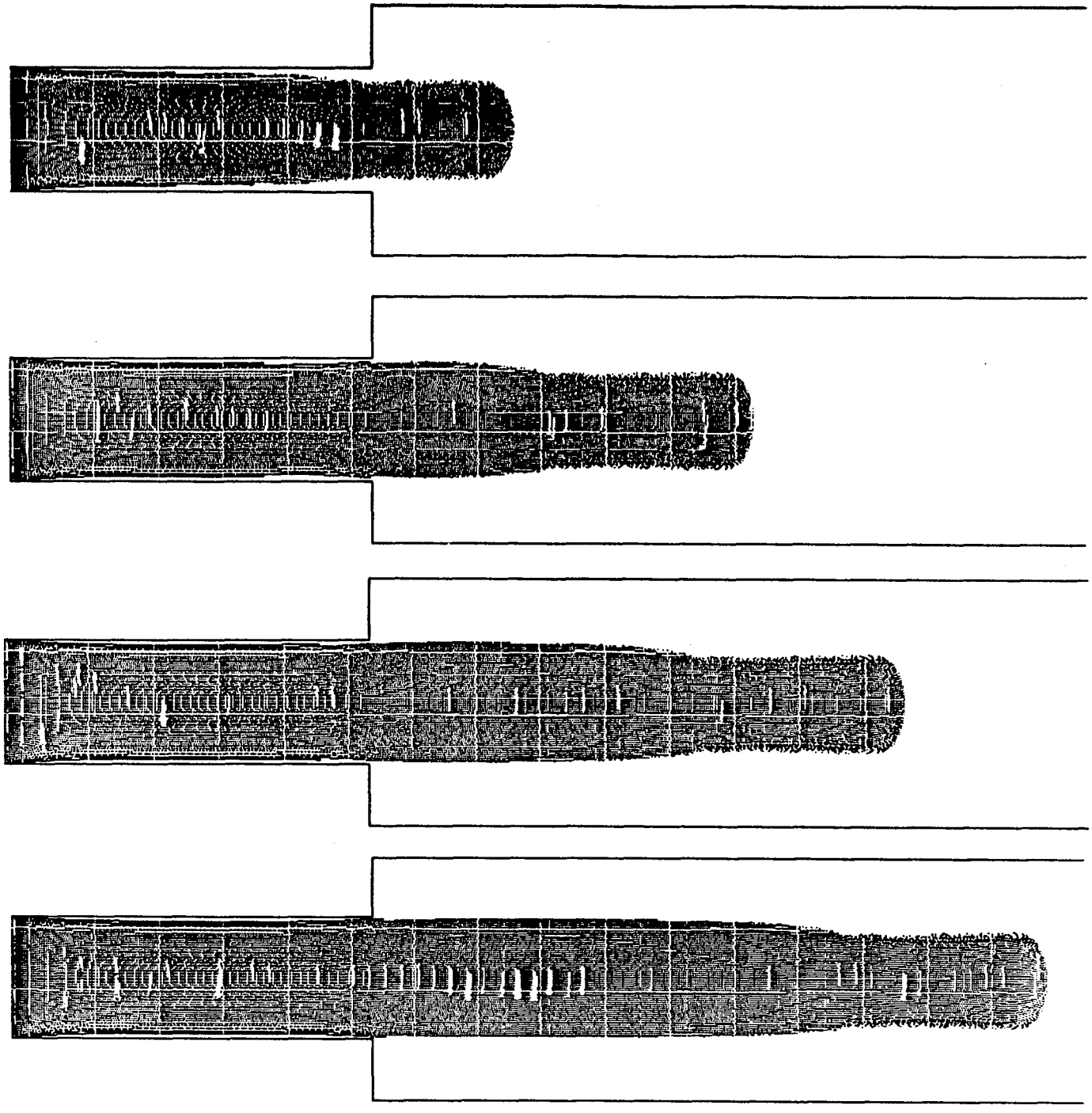

Fig. 15. Dieswell of a Generalized fluid at differents times for the case of K = 1.5. **a: t = 3.750, b: t = 5.625, c: t = 6.875, d: t = 8.125.**

5.2 Buckling of Newtonian and non-Newtonian Jets

To further demonstrate that the finite difference approach presented in this paper can deal with shear shinning viscosity, we present in this Section two calculations which simulates the buckling of thin viscous jets. This phenomenon has been investigated by several researchers in the past years (e.g. Cruickhank and Munson [14], Bejan [15]) and a two-dimensional theory explaining this instabillity has yet to be presented. Nevertheless, Cruickshank and Muson [14] and Cruickshank [16] have presented experimental and approximated results in order to predict jet buckling of planar and axisymmetric thin jets. In particular, it is postulated that for a planar jet, buckling will occur if the following restrictions are satisfied:

$$Re > 0.56 \quad \text{and} \quad L/D > 3\pi$$

where Re is the Reynolds number based on the slit width D and L is the height of the inlet to the plate.

For a Newtonian jet the Reynolds number is an important factor which dictates the behaviour of the flow whereas for a non-Newtonian jet it is changing locally according to the shear rate. To illustrate that the shear rate has a dominant effect on the buckling phenomenon we present two calculations which satisfy the conditions given above but the results for the shear thining jet is "different" from the corresponding Newtonian jet. The first calculation shows a thin jet which is injected into a square cavity (see figure 16) with the no-slip condition imposed at its walls. The cavity size is 5 cm by 5 cm and the inlet size is 4 mm. The inlet velocity was taken to be $U = 0.5\ m/s$ and the parameters defining the viscosity were

$$\begin{aligned} \nu_\infty &= 0.001\ m^2/s, \\ \nu_0 &= 0.010\ m^2/s, \\ m &= 1.0\ , \\ K &= 4.0\ . \end{aligned}$$

This gives a Reynolds number of $Re = 0.2$ ($Re = UD/\nu_0$) and $1/F_r^2 = 0.1570$.

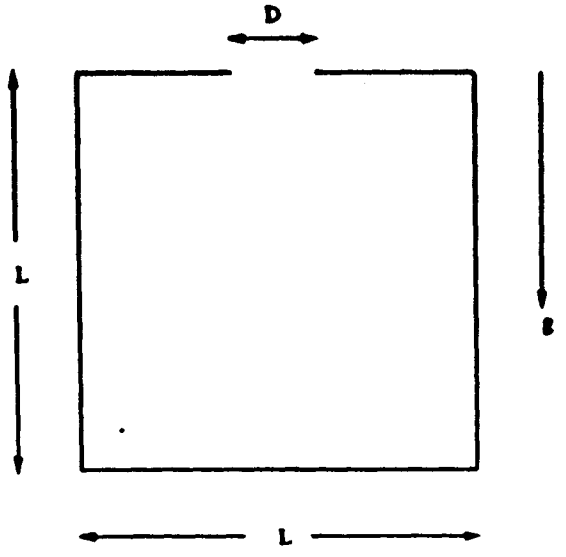

Fig. 16. Square cavity.

Figure 17 displays the fluid configuration plots at differents times with the corresponding Newtonian case.

a

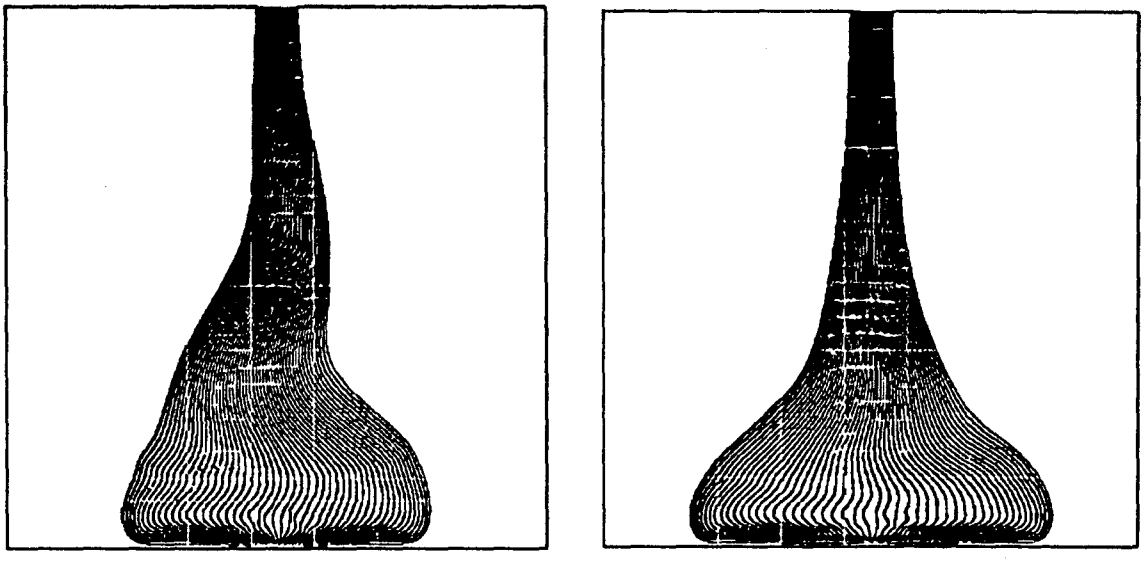

t = 40.625

b

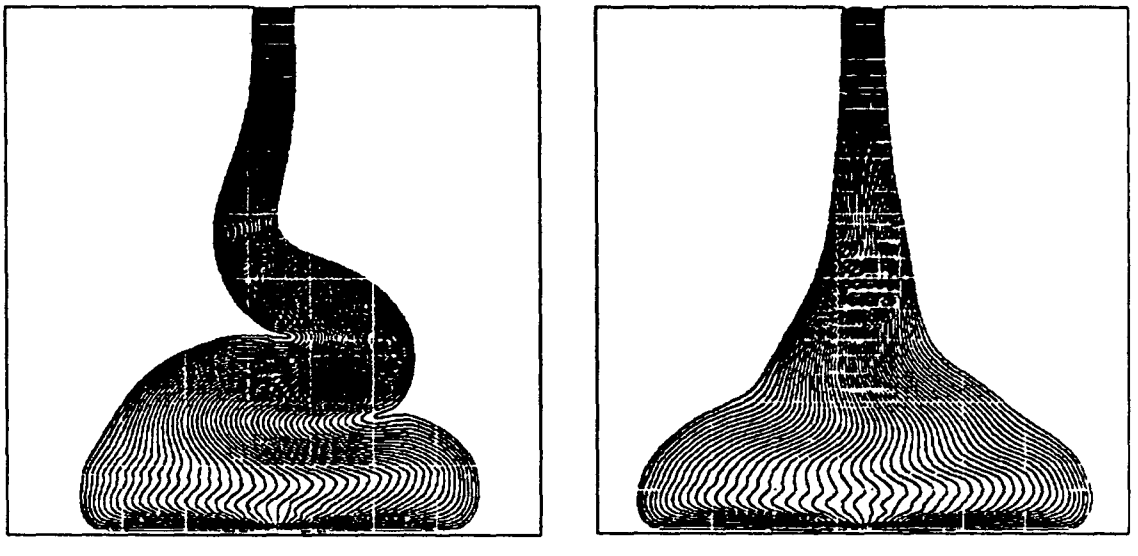

t = 50.000

Fig. 17. Buckling of a Newtonian (on the left) and non-Newtonian (on the right) Jets at different times.

c

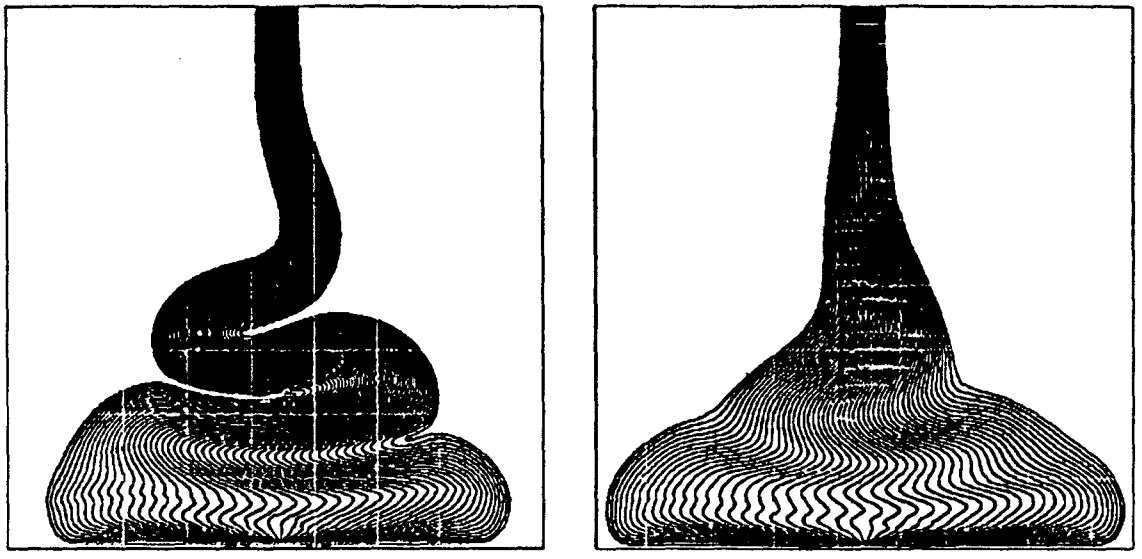

t = 56.250

d

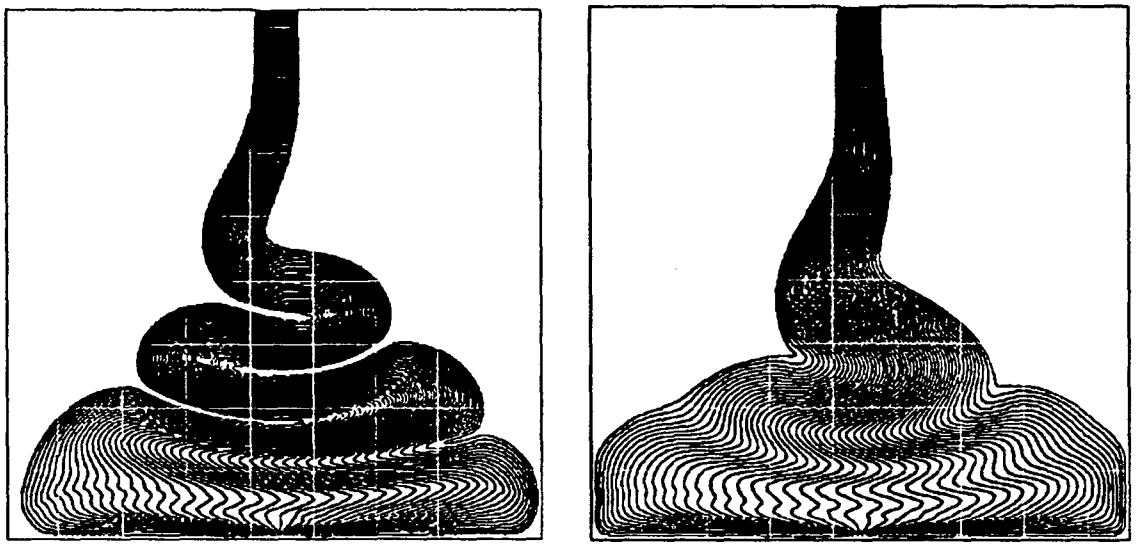

t = 62.500

Fig. 17. Continued.

The second calculation shows a thin jet injected into a rectangular cavity. The fluid properties are defined by

$$\nu_\infty = 0.001\ m^2/s,$$

$$\nu_0 = 0.050\ m^2/s,$$

$$m = 1.0\,,$$

$$K = 3.0\,.$$

The inlet width is $D = 5\ mm$ and the inlet velocity is $0.5\ m/s$. This gives a Reynolds number of $Re = 0.5$ and $1/F_r^2 = 0.1962$ and slenderness ratio of $H/D = 18.0$. Thus, according to Cruickshank's analysis the Newtonian jet would buckle. We have run the GENSMAC code for both Newtonian and shear thining fluids and the results are displayed in figure 18.

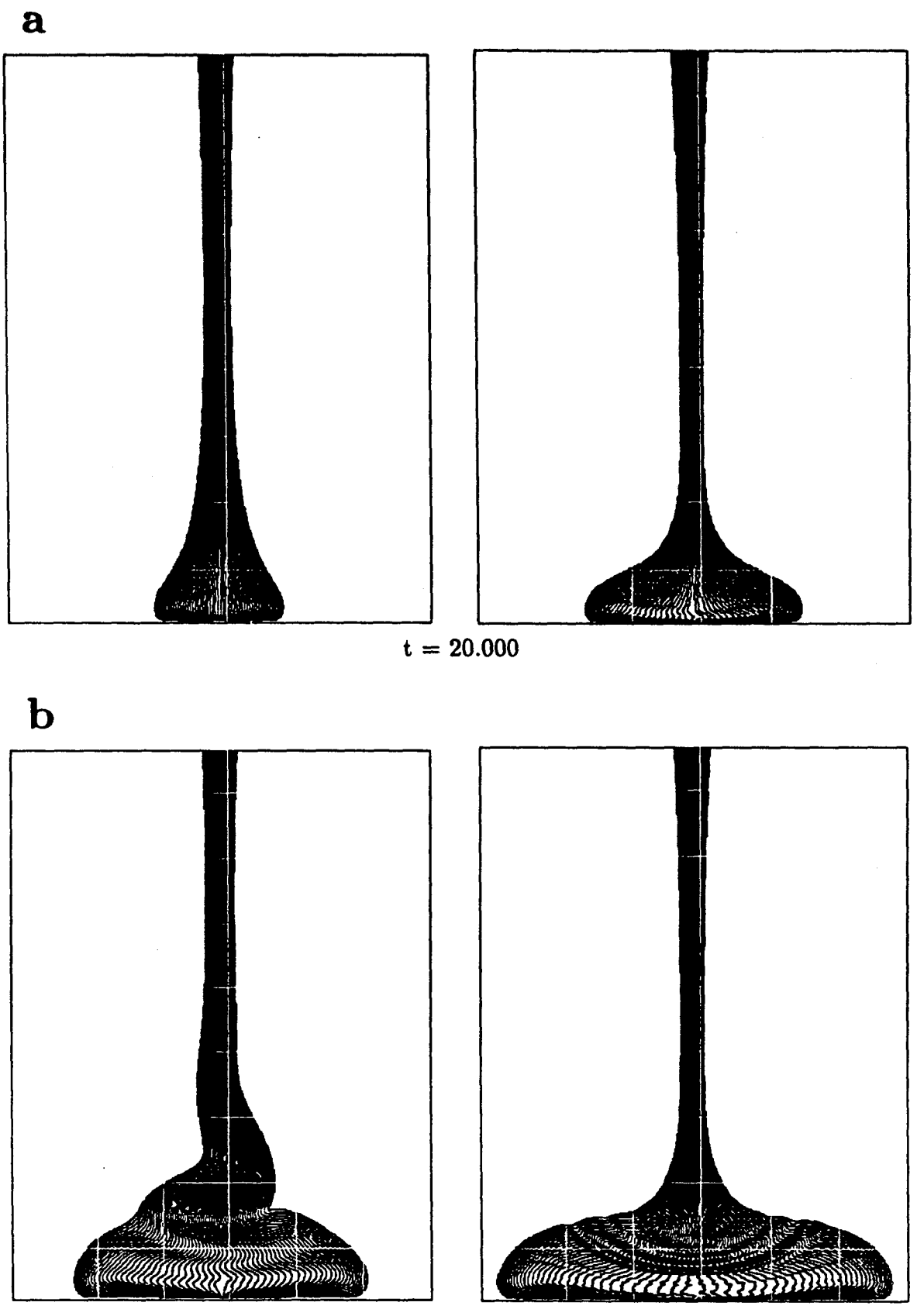

Fig. 18. Jet buckling of Newtonian (on the right) and non-Newtonian (on the left) jets. Flow visualization at different times.

c

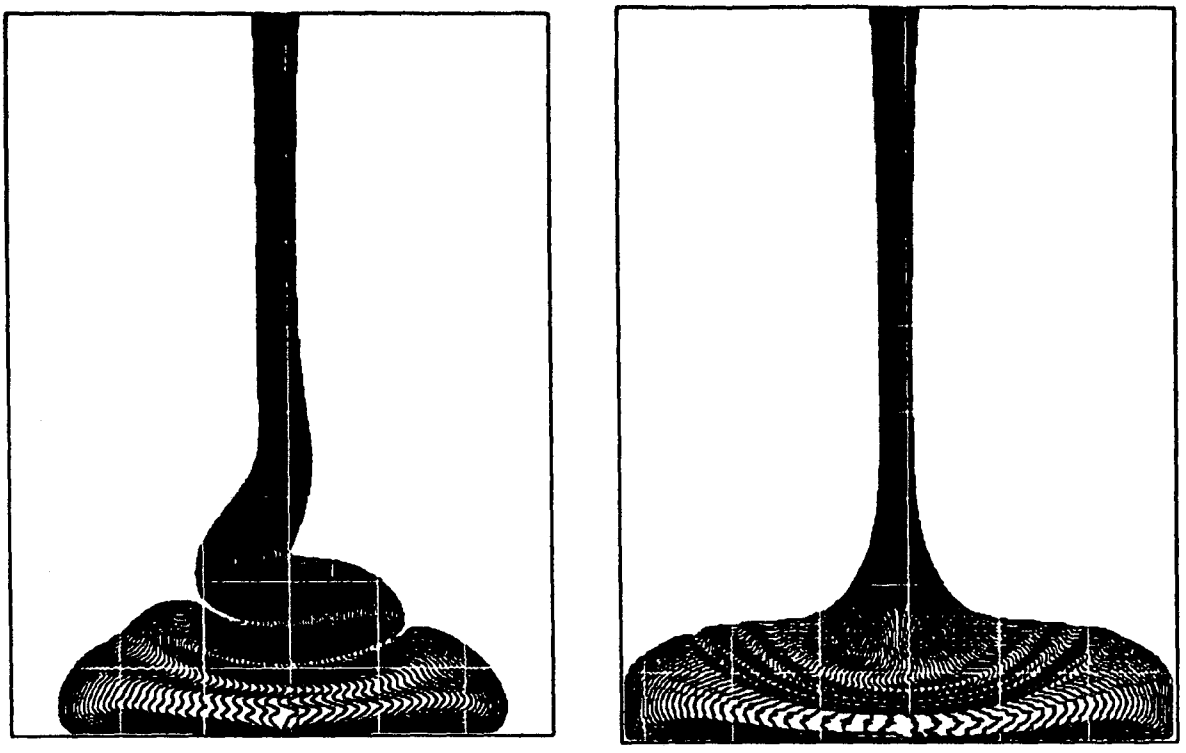

t = 41.269

d

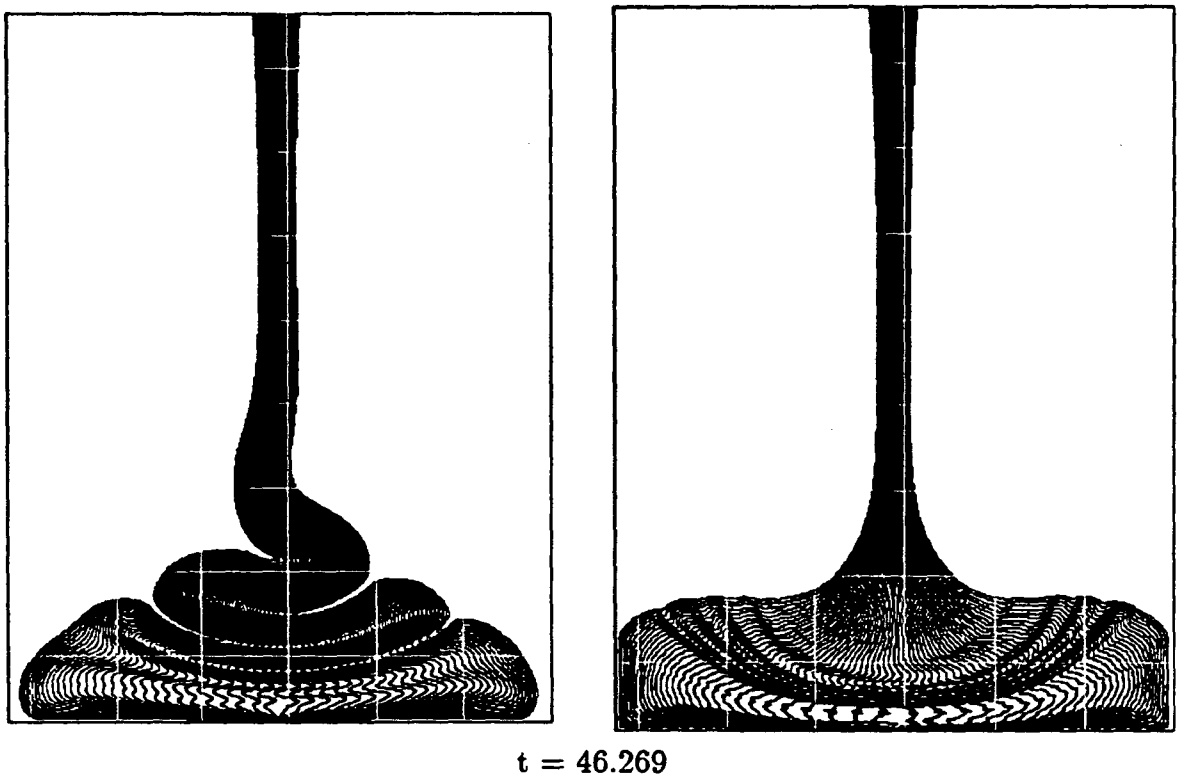

t = 46.269

Fig. 18. Continued.

5.3 Simulation of a Moulding Process in Complex Geometry

The third calculation presents the mould filling behaviour of the "foot" mould which is normally used in the manufacture of novelty products. The simulation described here shows the high speed injection moulding of relatively large cavities through small inlet ports. The product material (usually molten plastic, liquid metal, etc) enters the cavity at a high velocity as a free jet impinging on the surface mould opposite the inlet port. The material rheology is known to be shear thinning viscosity and the Reynolds number which is based on the inlet size and inlet velocity is typically small whereas the Froude number is large showing that the effect of gravity is negligible. Due to the complexity of the mould and the high curvature of the domain a fine mesh was employed. The geometry of the mould is shown in figure 19.

The fluid properties were taken to be

$$\nu_0 = 0.050\ m^2/s$$

$$\nu_\infty = 0.001\ m^2/s$$

$$K = 2.0$$

$$m = 1.0$$

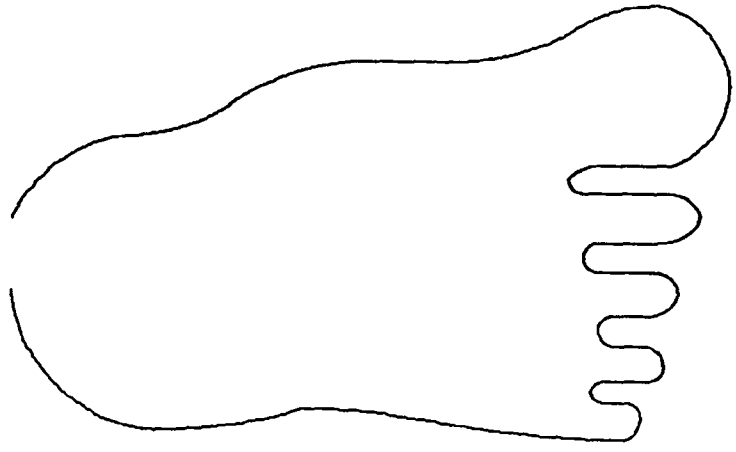

Fig. 19. Foot Mould.

The scaling parameters were the inlet velocity $U = 5\ m/s$ and the inlet size $D = 0.01\ m$ which gives a Reynolds number of $Re = 1.0$. A mesh of 6200 cells were employed and gravity was neglected as $(1/F_r^2) \approx 10^{-3}$. The results are displayed in figure 20 together with the respective Newtonian case.

a

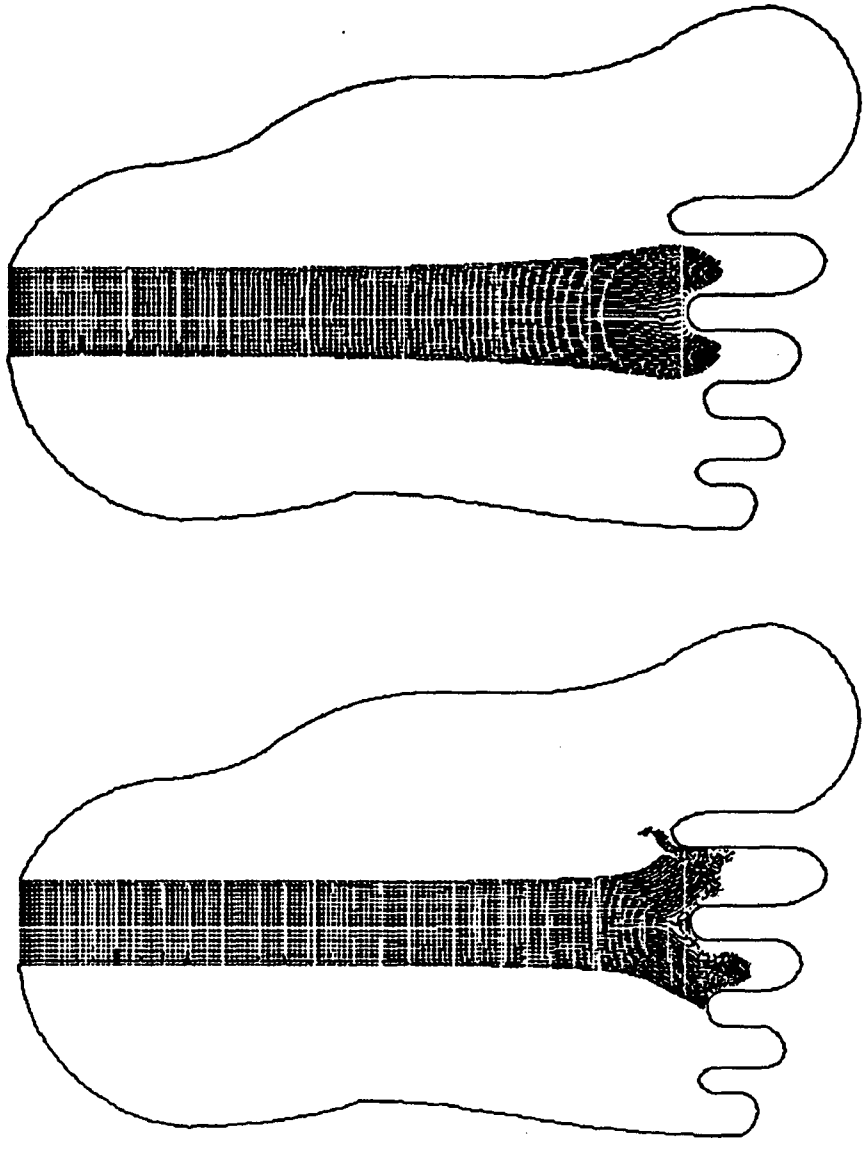

t = 9.000

Fig. 20. Simulaltion of the injection moulding for the "Foot" mould at different times. Newtonian (on the right) and non-Newtonian (on the left).

b

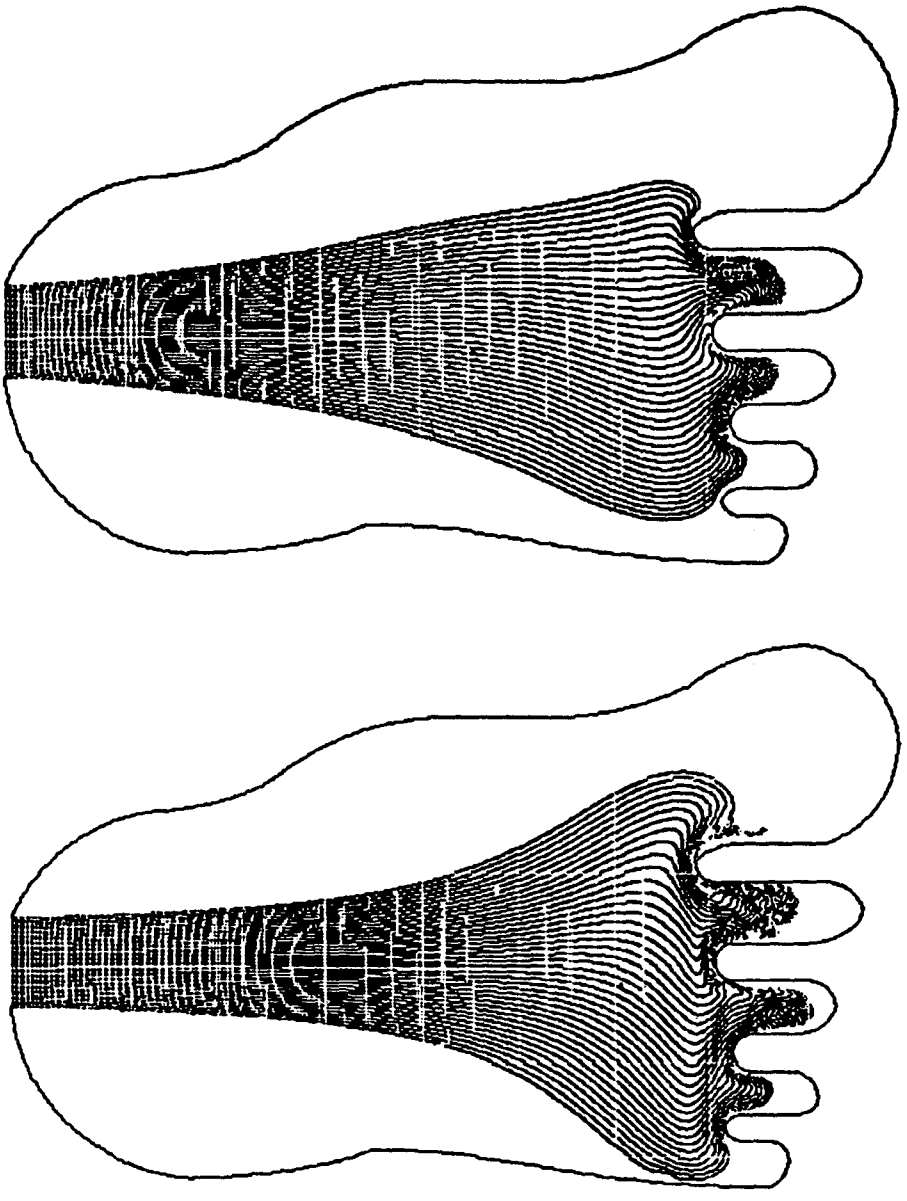

t = 18.000

Fig. 20. Continued.

c

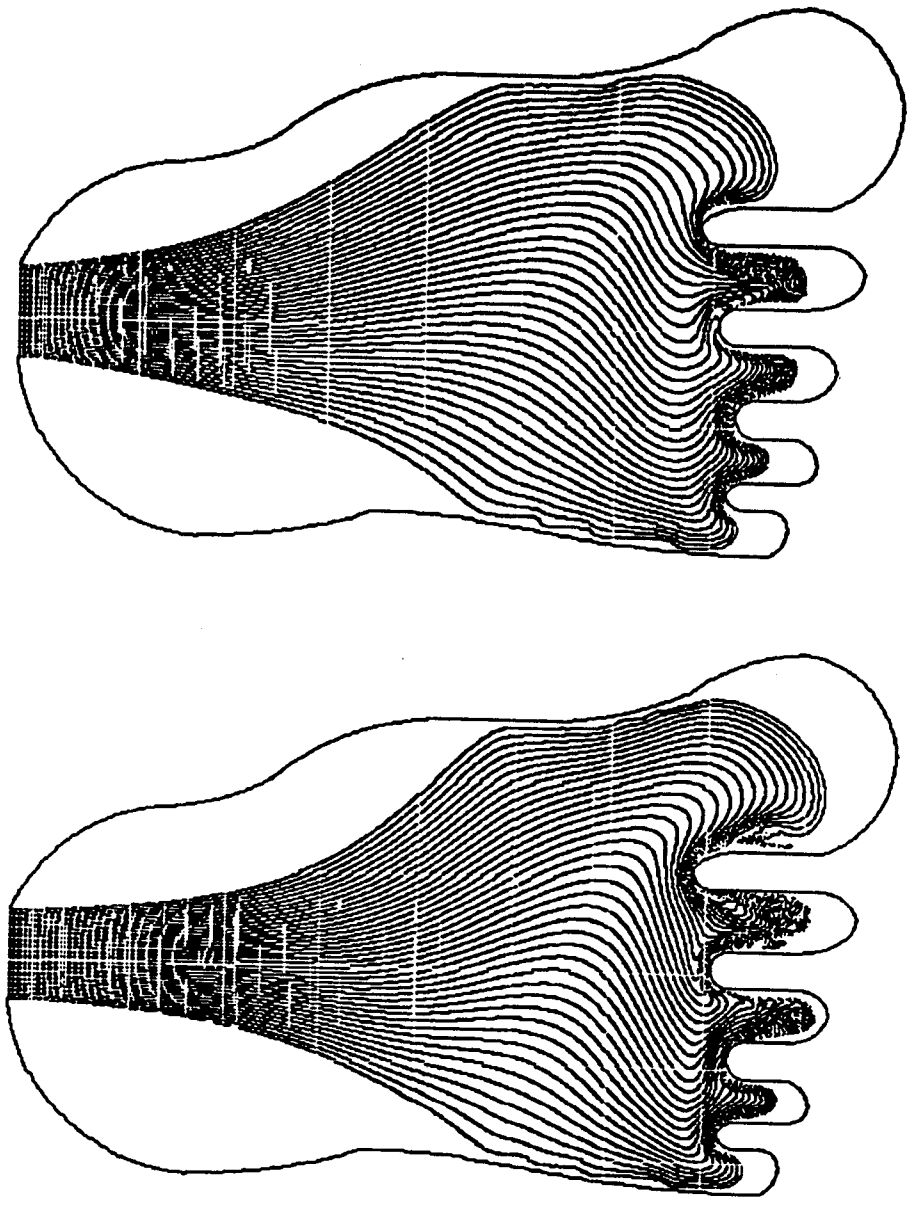

t = 27.000

Fig. 20. Continued.

ACKNOWLEDGEMENTS

The first author (M. F. Tome) would like to aknowledge the financial support of FAPESP - Fundação de Amparo a Pesquisa do Estado de São Paulo and CNPq - Conselho Nacional de Desenvolvimento Cientifico e Tecnológico for the development of this work.

References

[1] J. E. Welsch, F. H. Harlow, J. P. Shannon and B. J. Daly, (1966), "The MAC Method", Los Alamos Scientific Laboratory Report LA-3425, Los Alamos, New Mexico.

[2] A. Amsden and F. H. Harlow, (1970), "The SMAC method: A Numerical Technique for Calculating Incompressible Fluid Flows", Los Alamos Scientific Laboratory, Report LA-4370, Los Alamos, New Mexico.

[3] H. Miyata, (1986), *Finite-Difference Simulation of Breaking Waves*, J. Comp. Phys., 65, 179,214.

[4] J. A. Viecelli, (1969), *A Method for Including Arbitrary External Boundaries in the MAC Incompressible Fluid Computing Technique*, J. Comp. Phys., 4, 543-551.

[5] C. W. Hirt and J.P. Shannon, (1968), *Free-Surface Stress Conditions for Incompressible-Flow Calculations*, J. Comp. Phys., 2, 403,411.

[6] M. F. Tome and S. McKee, (1994), "GENSMAC: A Computational Marker-and-Cell Method for Free Surface Flows in General Domains", J. Comp. Phys., to appear; M. F. Tome, (1993), "GENSMAC: A Multiple Free Surface Fluid Flow Solver", Ph.D. Thesis, University of Strathclyde, Department of Mathematics, Glasgow, U.K.

[7] H. A. Barnes, J. F. Hutton and K. Walters, (1989), "An Introduction to Rheology", (Amsterdan: Elsevier, In Press).

[8] M. J. Crochet and R. Keunings, (1980), *Die Swell of a Maxwell Fluid: Numerical Prediction*, J. Non-Newtonian Fluid Mech., 7, 199.

[9] C. J. Coleman, (1977), *A note on the stich slip and die-swell problems for a second order fluid*, J. Non-Newtonina Fluid Mech., 3, 288.

[10] B. J. Omodei, (1980), *On the die swell of an axisymmetric Newtonian Jet*, Computers and Fluids, 8, 275.

[11] T.-J. Liu, T.-A. Yu and S.-H. Cheng, (1991), *Finite difference Solution of a Newtonian Jet Swell Problem*, Int. J. Num. Meth. Fluids, 12, 125-142.

[12] M. J. Crochet and R. Keunings, (1982), *Finite Element Analysis of a Die Swell of a Highly Elastic Fluid*, J. Non-Newtonian Fluid Mech., 10, 339.

[13] Y.-C. Ahn and M. E. Ryan, (1991), *A Finite Difference Analysis of the Extrudate Swell Problem*, Int. J. Num. Meth. Fluids, 13, 1289-1310.

[14] J. O. Cruickshank and B. R. Munson, (1981), *Viscous fluid buckling of plane and axisymmetric jets*, J. Fluid Mech., **113**, 221-239.

[15] A. Bejan, (1987), *Buckling flows: a new frontier in fluid mechanics*, Ann. Rev. Numer. Fluid Mech. Heat Transfer, **1**, 262.

[16] J. O. Cruickshank, (1988), *Low-Reynolds-number instabilities in stagnating jet flows*, J. Fluid Mech, **193**, 111-127.

NOTAS DO ICMSC

Serie computaçao

Nº 008/94 TOME, M.F.; DUFFY, B. GENSMAC: a numerical method for solving unsteady non-newtonian free surface flows

Nº 007/94 TOME, M.F.; MCKEE, S. Numerical simulation of viscous fluid: buckling of planar jets

Nº 006/94 MASIERO, P.C.; OLIVEIRA, M.C.F.; GERMANO, F.S.R; PIERRI,G.
Authoring and searching in dynamically growing hypertext data bases

Nº 005/94 NICOLETTI, M.C.; MONARD, M.C. Limiting the background knowledge in inductive logic programming

Nº 004/93 NICOLETTI, M.C.; MONARD, M.C. Learning horn clauses using the ILP system GOLEM

Nº 003/93 ARENALES, M.N.; MORABITO, R.N. An and/or graph approach to the solution of two-dimensional non-guillotine cutting problems

Nº 002/93 NICOLETTI, M.C.; MONARD, M.C. Herbrand interpretation model and least model within the framework of logic programming

Nº 001/93 MORABITO, R.; ARENALES, M.N. An and/or graph approach to the container loading problem